

Northumbria Research Link

Citation: Ashraf, Sahrish, Sultan, Muhammad, Bahrami, Majid, McCague, Claire, Shahzad, Muhammad Wakil, Amani, Mohammad, Shamshiri, Redmond R. and Ali, Hafiz Muhammad (2021) Recent progress on water vapor adsorption equilibrium by metal-organic frameworks for heat transformation applications. *International Communications in Heat and Mass Transfer*, 124. p. 105242. ISSN 0735-1933

Published by: Elsevier

URL: <https://doi.org/10.1016/j.icheatmasstransfer.2021....>
<<https://doi.org/10.1016/j.icheatmasstransfer.2021.105242>>

This version was downloaded from Northumbria Research Link:
<http://nrl.northumbria.ac.uk/id/eprint/46550/>

Northumbria University has developed Northumbria Research Link (NRL) to enable users to access the University's research output. Copyright © and moral rights for items on NRL are retained by the individual author(s) and/or other copyright owners. Single copies of full items can be reproduced, displayed or performed, and given to third parties in any format or medium for personal research or study, educational, or not-for-profit purposes without prior permission or charge, provided the authors, title and full bibliographic details are given, as well as a hyperlink and/or URL to the original metadata page. The content must not be changed in any way. Full items must not be sold commercially in any format or medium without formal permission of the copyright holder. The full policy is available online: <http://nrl.northumbria.ac.uk/policies.html>

This document may differ from the final, published version of the research and has been made available online in accordance with publisher policies. To read and/or cite from the published version of the research, please visit the publisher's website (a subscription may be required.)

1
2
3
4
5
6
7
8
9
10
11
12
13
14
15
16
17
18
19
20
21
22

Recent progress on water vapor adsorption equilibrium by metal-organic frameworks for heat transformation applications

**Sahrish Ashraf ^a, Muhammad Sultan ^{a,b,*}, Majid Bahrami ^b, Claire McCague ^b,
Muhammad W. Shahzad ^c, Mohammad Amani ^b, Redmond R. Shamsiri ^d, Hafiz M. Ali ^e**

^a Laboratory for Energy and Env. Engineering Research, Department of Agricultural Engineering, Bahauddin Zakariya University, Bosan Road, Multan 60800, Pakistan

^b Laboratory for Alternative Energy Conversion (LAEC), School of Mechatronic Systems Engineering, Simon Fraser University, Surrey, BC, Canada

^c Mechanical and Construction Engineering Department, Northumbria University, Newcastle Upon Tyne NE1 8ST, UK

^d Leibniz Institute for Agricultural Engineering and Bioeconomy, Max-Eyth-Allee 100, 14469 Potsdam-Bornim, Germany

^e Department of Mechanical Engineering, King Fahd University of Petroleum and Minerals, Dhahran, Saudi Arabia

* Corresponding Author: Prof. Muhammad Sultan, Dr.Eng.

Emails: muhammadsultan@bzu.edu.pk ; muhammad_sultan@sfu.ca

Tel: +92-333-6108888; Fax: +92-61-9210298

23 **Abstract**

24 Adsorption-based heat transformation systems are studied from the twentieth century;
25 however, their performance is low to replace conventional systems. Metal-organic frameworks
26 (MOFs) are providing a new class of micro- and nano-porous organic adsorbents. These have
27 adjustable geometry/topology with a large surface area and pore volume. A comparison of the
28 coefficient of performance (COP) between the MOFs and conventional adsorbents-based cooling
29 systems is made for the years 1975-2020. Conventional adsorbents achieve COP of 0.85, whereas
30 it is improved to 2.00 in the case of MOFs. The main bottleneck in the lower COP level is the low
31 adsorption equilibrium amount. This study is aimed to provide comprehensive detail of water-
32 vapor adsorption equilibrium and physicochemical properties of hydrophilic MOFs. Zn based
33 MOFs are not stable in the presence of water-vapors, whereas MIL series, Zr, Ni, and Cu based
34 MOFs are relatively more stable. Among the studied MOFs, MIL-101(Cr) possesses the highest
35 adsorption uptake of 1.45 kg/kg at 25°C (saturation condition) and outperformed for heat
36 transformation applications. Its uptake can be increased to 1.60 kg/kg by coating with graphite
37 oxide. For water desalination, MIL-53(Al) exhibits specific daily water production of 25.5
38 m³/ton.day (maximum) with a specific cooling power of 789.4 W/kg. Both MIL adsorbents are
39 found promising which can be considered for various adsorption applications.

40 **Highlights**

- 41 • An insight is provided on MOFs suitability for heat transformation applications
42 • Physical/crystal properties of MOF/water pairs are reviewed and compared
43 • High-uptake MOFs are explored for cooling, air-conditioning and desalination
44 • Adsorption equilibrium data are compared, and isotherm models are discussed

45 **Keywords:** MOFs; water vapors adsorption equilibrium; cooling; air-conditioning;
46 desalination.

47 **List of abbreviations**

48	A	adsorption potential [kJ/kg]
49	AlFs	aluminum fumarate
50	b	constant of Sips adsorption model [-]
51	BET	Brunauer-Emmett-Teller
52	COP	coefficient of performance [-]
53	COP _h	coefficient of performance of heating [-]
54	COP _{ref}	coefficient of performance of refrigeration [-]
55	D-A	Dubinin-Astakhov
56	DAC	desiccant air-conditioning
57	DE	dehumidification effectiveness
58	DSLIF	dual site langmuir-freundlich
59	DUT	Duban University of Technology
60	DW	desiccant wheel
61	E	activation energy [kJ/kg]
62	GO	graphite oxide
63	H	constant of Freudlich adsorption model [kg/kg]
64	IUPAC	International Union of Pure and Applied Chemistry
65	MCHE	MOF coated heat exchanger
66	MIL	Material Institute Lavoisier
67	MOF	metal-organic framework
68	n	D-A model constant [-]
69	P	vapor pressure [kPa]
70	P/P _o	relative pressure [-]
71	PHCM	precise humidity control material
72	P _o	saturated vapor pressure [kPa]
73	P-T-W	pressure-temperature-concentration
74	R	general gas constant [kJ/kg.K]
75	RH	relative humidity [-] or [%]
76	SCHE	SGB coated heat exchanger
77	SCP	specific cooling power [W/kg]
78	SDWP	specific daily water production [ton/day/ton-ads]
79	SEM	scanning electron microscopy
80	SHG	second-harmonic generation
81	T	temperature [°C, K]
82	T _{con}	temperature of condenser [°C] or [K]
83	T _{eva}	temperature of evaporator [°C] or [K]
84	T _{in}	inlet temperature [°C] or [K]
85	UiO	University of Oslo
86	w	adsorption uptake [kg/kg]
87	w ^o	maximum adsorption uptake [kg/kg]
88	η _{deh}	dehumidification effectiveness [-]
89		

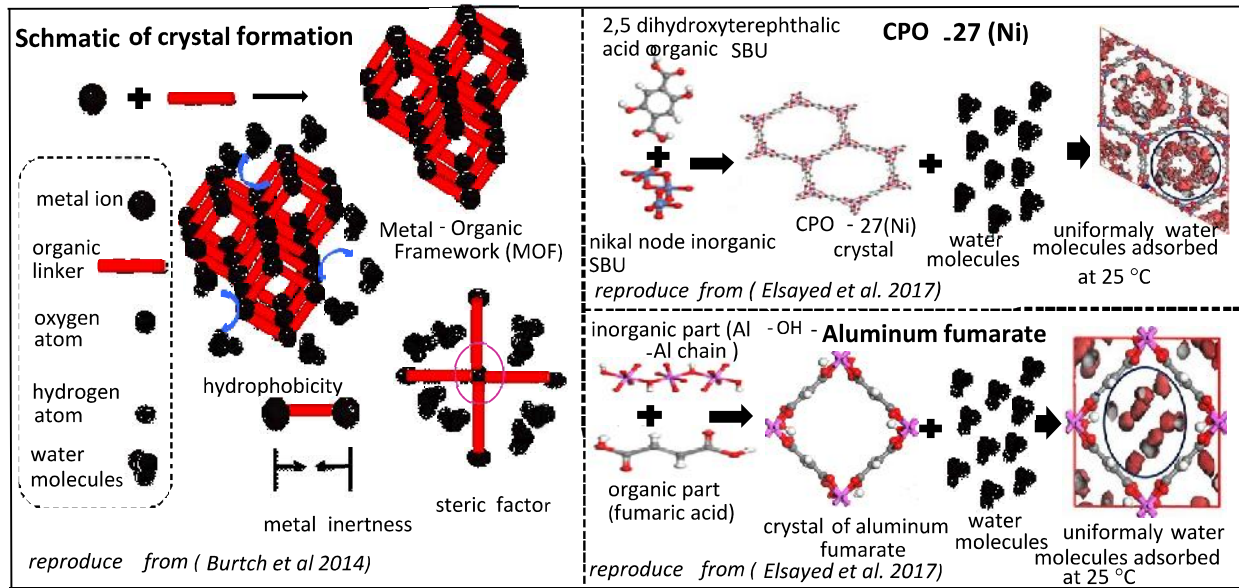
90 1. Introduction

91 Adsorption cooling and air-conditioning systems could be energy-efficient solutions for
92 various applications compared to conventional technologies [1,2]. The performance of these
93 systems is directly linked with adsorbent-adsorbate interactions [3,4] and the type of adsorption
94 isotherms [5–7]. Thereby, the adsorbents' structure has a significant role in developing useful
95 technologies [8,9]. Various adsorbent-adsorbate pair have been studied in the literature [10–12].
96 In this regard, the highest uptake was recorded by adsorption of difluoromethane (HFC-32) onto
97 phenol resin-based adsorbent [13]. Water vapor adsorption has been studied for various adsorbents
98 [14,15] e.g. silica-gel [16–18], activated carbon [19,20], polymers [21–24] and zeolite [25–28].
99 These hydrophilic adsorbents are investigated for many applications e.g. silica-gel for greenhouse
100 air-conditioning [29], drying of agricultural products [30,31], thermal energy storage system [32],
101 and adsorption cooling/air-conditioning [16,33]; activated carbons and silica gel for greenhouse
102 air-conditioning [29], adsorption refrigerator [34,35], air-conditioning [36], and ice-making [37];
103 polymers for desiccant air-conditioning (DAC) [38]; and zeolites for heat storage [26] and air-
104 conditioning [39,40]. The adsorbents' hydrophobicity is greatly concerned with surface area and
105 volume of macro-, meso-, micro and nano-pores to welcome incoming molecules of water-vapors
106 [41]. In this regard, metal-organic frameworks (MOFs) are a new class of micro- and nano-porous
107 adsorbents with exclusive adsorption properties [14,42]. These are known as porous coordination
108 polymers, metal-organic materials and organic coordination polymers [43–46].

109 The MOFs are hybrid adsorbents in which organic linkers connect with inorganic metal ions
110 by coordination; metal ions provide more stability to crystals and enhance their hydrophilic
111 character. Metal nodes in MOFs increase flexibility and side spaces [49], providing many ways to
112 synthesize many adsorbents with the same organic linker. According to the Cambridge database
113 [47], nearly 12,000 MOF structures have been synthesized until now using 102 organic linkers
114 with different metal nodes. They have a more flexible structure design with the greater ability to
115 control pore functionalization than other organic adsorbents like zeolite and polymers.
116 Furthermore, the MOFs have an organic part in their solid structure formation, making them more
117 versatile than zeolite [48]. A simple schematic of the MOFs formation is shown in Fig. 1. It can
118 be observed that MOFs crystal formed cage-like 3-dimensional open-spaced structure due to the
119 support of metal ions and possess huge accessible free space to attract water molecules. A simple
120 schematic of crystal formation and adsorption of water-vapor for CPO-27(Ni) and aluminium

121 fumarate (AIFs) is also shown in the figure. It can be observed that these adsorbents possess more
122 fluctuations in structure and crystal design while interaction with water vapors. Many experimental
123 studies showed that MOFs had higher water-vapor uptake than conventionally used adsorbent, e.g.
124 silica-gel [49,50]. There is a functional relationship between the adsorbent structure and the
125 amount of adsorption equilibrium investigated in the literature [51–53]. Moreover, the surface
126 area, pores volume, and structural stability of the MOFs may significantly affect the water-vapor
127 adsorption equilibrium [54–56]. Water-vapor adsorption uptake can be improved by coating the
128 adsorbents with other metal(s) [57]. For example, adsorption uptake of MIL-101(Cr) has increased
129 1.07 times when coated with graphite oxide (GO) at 25°C and 0.90 relative pressure, as its surface
130 area increased from 2489 to 3522 m²/kg [58–60].

131 Various studies has been conducted to synthesized and characterized the MOFs in term of
132 water-vapor adsorption equilibrium e.g. MOF-5 [43,61,62], HKUST-1 [56,63], CPO-27(Ni, Cr,
133 Cd, Mg) [49,52,53,64,65], MIL-(101, 100, 125) [54,66,67] and zirconium-based MOFs [68,69].
134 Therefore, this study aims to provide a brief comparison of the MOF adsorbents that can be helpful
135 in selecting a suitable adsorbent according to thermophysical and thermodynamic properties.
136 Several studies on MOFs/adsorbates interaction have been reported in the literature using close
137 and open-cycle adsorption cycles [70] for cooling [71–74] and air-conditioning [53,60]
138 applications. In the case of open-cycle applications, MOFs adsorption uptake is supposed to be
139 limited to water-vapors [60], whereas, in the case of close-cycle applications, MOFs adsorption
140 have been reported with various adsorbates, e.g. water-vapors [53,72], ethanol [75–77] and
141 methanol [73,78]. However, in each case, adsorption equilibrium uptake and adsorption kinetics
142 are key adsorption properties for developing a real system [79]. Adsorption uptake of ethanol onto
143 MIL-101 has been reported as high as 1.10 kg/kg (at 25°C) [77] and 0.74 kg/kg (at 25°C)) [75]
144 and methanol onto HKUST-1 and MIL-101 yielded 0.55 kg/kg (at relative pressure of 0.90) and
145 1.20 kg/kg (at relative pressure of 0.80), respectively [73]. Similarly, MOF yielded higher
146 methanol adsorption uptake and performance at lower heat rejection and evaporator temperature
147 than activated carbon. This higher adsorption uptake of ethanol significantly increases the
148 coefficient of performance (COP) and specific cooling power (SCP) of the systems. In each case,
149 MOFs possess higher cyclic stability e.g. MIL-101/ethanol stable after 60 adsorption/desorption
150 cycles [75] and MIL-101(Cr)/methanol can be applicable up to 1000 adsorption/desorption cycles
151 [73].



153

154 **Fig. 1.** Fundamental of MOFs crystal formation along with water-vapor interaction (left). The
 155 basic unit of crystal formation and change in crystal after water-vapor adsorption for CPO-27(Ni)
 156 (top right), and aluminium fumarate (bottom right), reproduced from [50,80].

157

158 Hydrophilic MOFs have been reported many close-cycle applications including water
 159 desalination [50,52,81], adsorption heat pump and adsorption chillers [49,55,82], heat
 160 transformation and storage [67,69,83,84], solar energy storage [85], humidity control [86],
 161 adsorption cooling and air-conditioning [53,71,72,87], pollutant removal [88], and ice-making
 162 [81]. In an experimental study [53], CPO-27(Ni) has 1.23 times higher water-vapor adoption
 163 uptake than silica-gel when investigated for automobile air-conditioning, resulting in COP and
 164 SCP of the system as 0.26 and 105 W/kg, respectively. Similarly, hydrophilic MOFs have been
 165 investigated for many open-cycle application, e.g. water harvesting [89,90], moisture sensing [91],
 166 wastewater treatment [92,93] and air-conditioning [60]. In a simulation study [60], MIL-101(Cr)
 167 investigated for open-cycle air-conditioning purposes and results showed that MIL-101(Cr)
 168 outperformed silica-gel.

169 In this regard, many studies have been reported in the literature to investigate the performance
 170 of these materials, highlighting their potential use in many applications. This study aimed to review

171 the water-vapor adsorption equilibrium of hydrophilic MOFs available in the literature and their
 172 potential to use for adsorption based cooling and air-conditioning applications.

173

174 **2. Adsorption characteristics of MOF/water pairs**

175 This study reviewed various kinds of MOF based hydrophilic adsorbents which were
 176 synthesized and characterized in the literature e.g. MIL-101 [50,83,94,95], MIL-53 [50,66,92,96],
 177 MIL-100 [97,98], MIL-125 [99,100], MIL-96 [101], MIL-127 [102], MIL-101 Cr/SrBr₂ [85],
 178 MOF-1 [103], MOF-5 [43,61,62,104], MOF-14 [105], HKUST-1/MOF-199 [55,56,63,104,106],
 179 CPO-27 [52,64,107–111], CAU-10-H [112], MOF-177 [104], Fe-BTC [55], MOF-801 [68],
 180 PIZOF [113,114], MOF-806 [68], UiO-66 [68,99,113,115–117], MOF-802 [68], MOF-88 [118],
 181 UiO-67 [117], MOF-808 [68], DUT-67 [69,119]. The details of the adsorbents are provided in Fig.
 182 2.

Metal-organic frameworks (MOFs)		
MIL series	Zirconium based	Others
MIL-101 [50,83,94,95]	MOF-801 [68]	CPO-27 [52,64,107–111]
MIL-53 [50,66,92,96]	PIZOF [113,114]	HKUST-1 [55,56,63,104,106]
MIL-100 [97,98]	MOF-806 [68]	Fe-BTC [55]
MIL-125 [99,100]	UiO-66 [68,99,113,115–117]	MOF-14 [105]
MIL-96 [101]	MOF-802 [68]	CAU-10-H [112]
MIL-127 [102]	MOF-88 [118]	MOF-177 [104]
MIL-101 Cr/SrBr ₂ [85]	UiO-67 [117]	MOF-1 [103]
	MOF-808 [68]	MOF-5 [43,61,62,104]
	DUT-67 [69,119]	

183

184 **Fig. 2.** Overview of the MOF adsorbents studied in the literature.

185

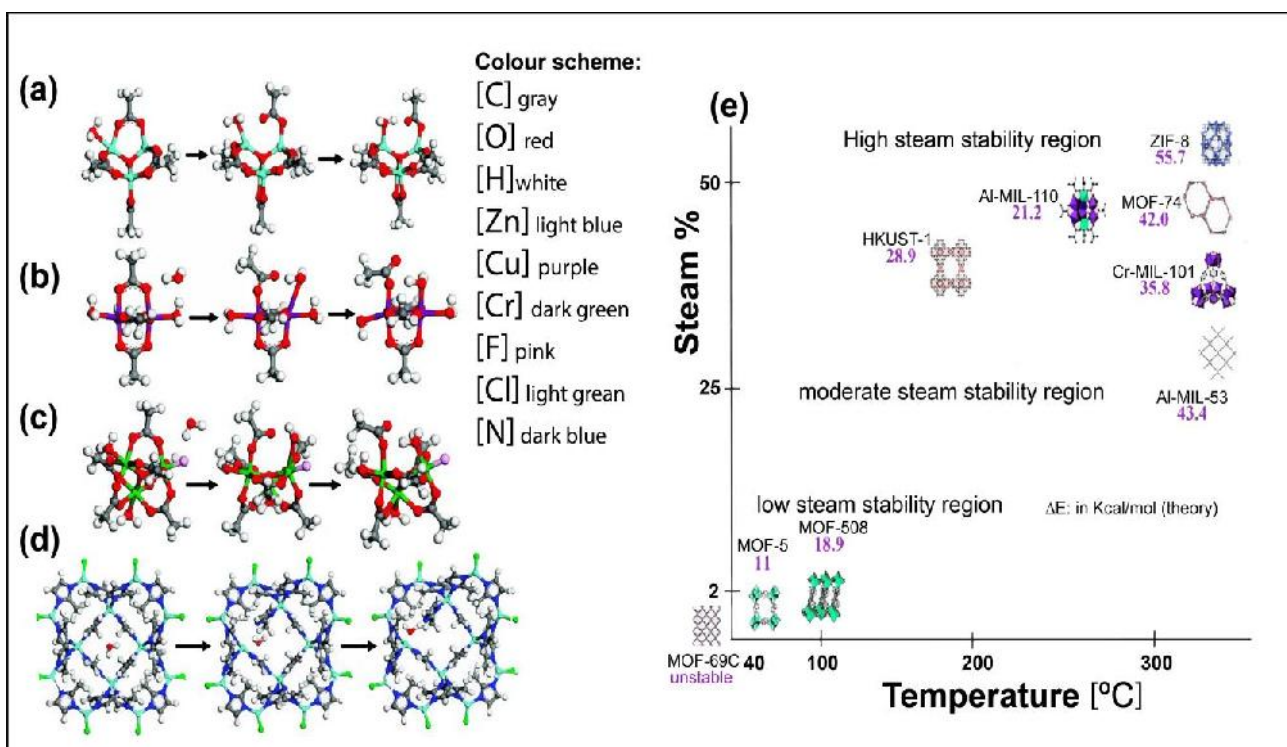
2.1. Physical characteristics and chemistry

The MOFs are formed by the coordination of organic linkers and metal ions. These metal ions act as a base, while organic linker act as a bridging unit. The strong coordination between metal ions and organic linkers is a key factor to make a stable crystal. The crystal stability makes these adsorbents more versatile and unique than other adsorbents. Crystal and structural properties of MOFs based adsorbents with good water vapors adsorption uptake are shown in Table 1. Many crystals have uniformly connected each other to form a huge molecule with empty spaces. However, the presence of empty spaces on each side makes these adsorbents more reactive and unstable. They can easily react to chemicals and moisture present in the air during their preparation process. Therefore, it is necessary to achieve control conditions in the laboratory during their preparation. Water molecules get attached to the crystals when these adsorbents are completely synthesized. Heat treatment is required to remove excessive water molecules from the crystals [120]. This heat treatment inactivates the adsorbents and makes them more thermally and chemically stable, e.g. HKUST-1 and MIL-101 have thermal stability of 240°C and 275°C, respectively [63,95].

Various studies highlighted hydrophilic character and higher hydrothermal stability of these adsorbents, e.g. nickel-based CPO-27 [50,53,107]. Some of the MOFs may be hydrophobic and possessed a higher attraction for other adsorbate molecules. For example, MOF-5 is not moisture stable, but it can be utilized for gas separation applications [61]. The hydrophilic and hydrophobic character can be determined by the type of metal ions and nature of interaction with the organic linker and metal ions. Fig. 3(a)-(d) [128] gives a brief insight into the geometries of clusters transition states upon ligand hydrolysis/displacement reaction in MOF-5, HKUST-1, MIL-101 and ZIF-8, respectively. Besides, a simple water stability map of different MOFs materials is shown in Fig. 3(e) [121]. Some of the adsorbents of this class are moisture sensitive and degraded when exposed to water-vapors. It is because of the type of metal node, e.g. Zn metal-based MOFs are moisture sensitive [104]. Similarly, MOF-5 is not stable in the presence of moisture and degraded at a relative humidity (RH) of more than 4% [61]. Additionally, some of the adsorbents are stable at lower relative pressure range and start to degrade at high relative pressure, e.g. HKUST-1 (also known as CuBTC/MOF-199 [65]) is more moisture stable at lower relative pressure [56]. It is due to the presence of copper (Cu) metal ions which are moisture stable. The bond length (Cu-Cu bond) starts to elongate when water-vapors contact with its crystal [59], and bond length elongation

217 increases continuously when the number of water-vapour molecules increases. Therefore,
218 HKUST-1 shows relatively higher water-vapor uptake at lower relative pressure and unstable at
219 higher relative pressure. However, changing metal ions with the same organic linker can alter
220 adsorptive and physical characteristics. For example, MOF-74 [111], also known as CPO-27
221 [64,65], developed by the coordination of 2nd group transition metal ions (Mg, Ni, Cd, Cu and Cr)
222 with 2,5-dioxide-1,4-benzenedicarboxylate organic linker [64,107–109]. Moisture stability in CPO-
223 27 is determined by metal and oxygen (M-O) bond strength [122]. Bond length elongation is large
224 in the case of Cr, Cd, Mg and Cu metals. While the M-O bond elongation is negligible in Ni metal
225 ion and crystal retained its original position when it dehydrated. Hence, CPO-27(Ni) found to be
226 more stable in the presence of water-vapors [107].

227 Crystal formation/deformation in the presence of water-vapors in the MIL series is observed,
228 which is quite different from other studied MOFs adsorbents. Most of the MIL series's adsorbents
229 attracted fewer water-vapors at lower relative pressure ranges (0.10 to 0.30) compared to higher
230 relative pressure (0.50 to 0.90) [59,71,94]. For examples, MIL-101 and MIL-100 have started to
231 absorb water-vapors at relative pressure ranging from 0.30 to 0.40. Similarly, aluminium (Al) and
232 gallium (Ga) metal(s)-based MOFs were found to be water-vapor stable as compared to other metal
233 ions-based adsorbents. For example, AIFs [92] showed a honeycomb-like flexible structure with
234 more surface area due to long repeating (-Al-O-Al-O-Al-O-Al-) chains. Therefore, water-vapors
235 can easily attach to the crystal without deformation. Thus, the crystal retained their original
236 position when dehydrated or thermally treated. Similarly, zirconium (Zr)-based MOFs like UiO-
237 66 is formed from the octahedral group of $Zr_6O_4(OH)_4$ with BDC linker has possessed higher
238 moisture stability [123].



239


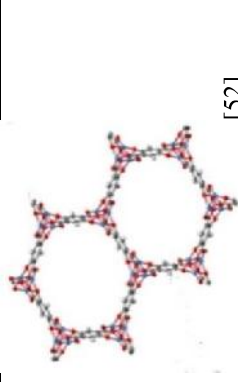
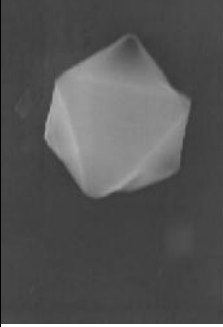
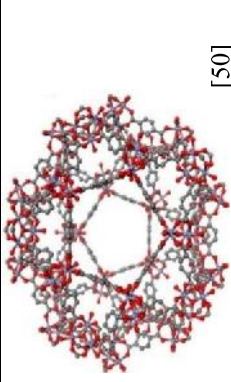
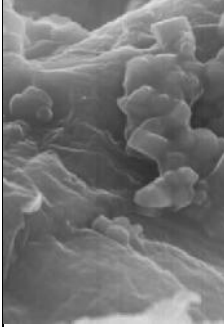
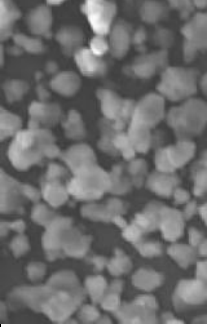
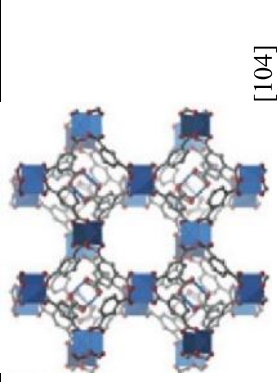
240

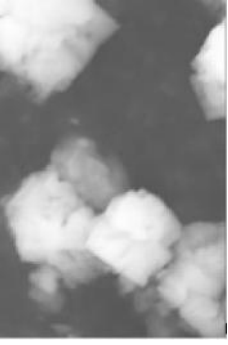
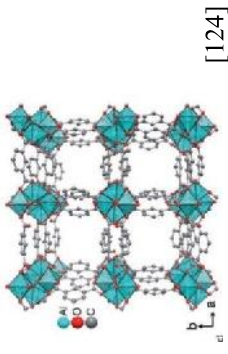
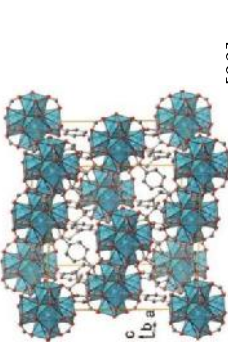
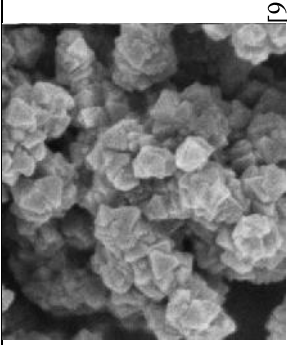
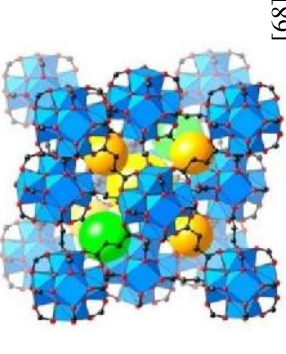
241

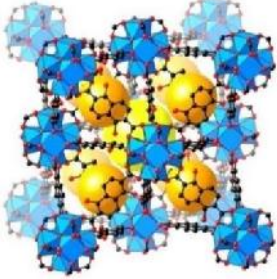
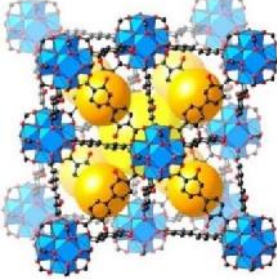
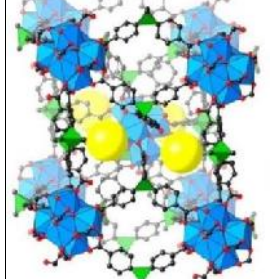
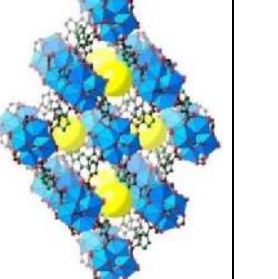
242


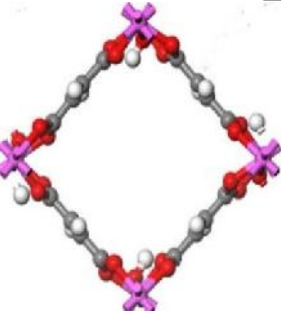
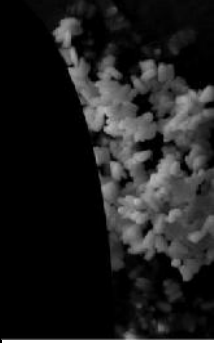
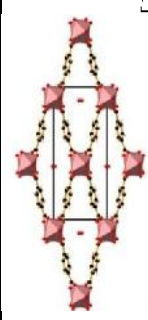

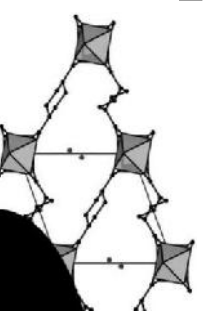
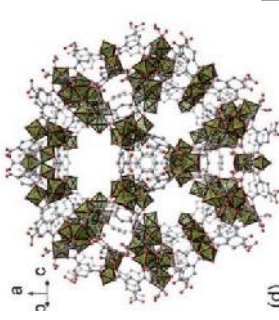
Fig. 3. A brief insight of the geometries of clusters transition states upon ligand hydrolysis/displacement reaction in (a) MOF-5, (b) HKUST-1, (c) MIL-101 and (d) ZIF-8; (e) a general stability sketch of MOFs in the presence of water molecules [121].

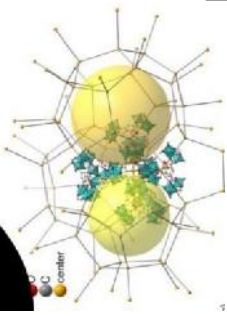
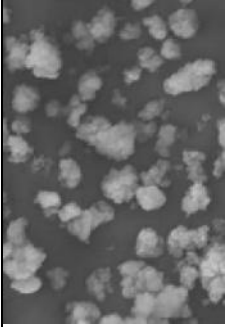
243 **Table 1.** Details about the structure and physical properties of the studied MOFs.

MOF class	MOF name	SEM or SHG image	Crystal structure	Chemical formula	Physical properties		Pores volume (cm ³ /g)
					Surface Area (m ² /g)		
					BET	Langmuir	
CPO-27/MOF-74	CPO-27 (Ni)	 [52]	 [52]	Ni ₂ (dhtp)(H ₂ O) ₈ ·8H ₂ O [107]	1113 [110] 1337 [108]	N/A	0.39 [110] 0.54 [108]
MIL-101	MIL-101-Cr	 [94]	 [50]	[Cr ₃ (O)(BDC) ₃ (F, OH)-(H ₂ O) ₂] [83]	4000 [83] 2789 [94]	4500-5500 [95]	1.51 [85]
Composite MIL-101(Cr)@GO	MIL-101(Cr)@GO-2	 [94]	N/A	N/A	3472 [94]	5031 [94]	1.69 [94]
HKUST-1/CuBTC/MOF-199	HKUST-1/CuBTC/MOF-199	 [55]	 [104]	C ₁₈ H ₆ CH ₃ O ₁₂ [55] Cu ₃ (C ₉ H ₃ O ₆) ₂ [104]	1500-2100 [55] 1568.5-2081.5 [106]	917.6 [63]	0.75 [106]

CAU-10	CAU-10-H	 [112]	 [124]	[Al(OH)(O ₂ C-C ₆ H ₄ -CO ₂)]·1.7H ₂ O:C 40.2 %, H 3.1% [112]	S _{BET} =635 [112]	N/A	0.23 [112]
Zirconium based MOFs	UiO-66	N/A	 [99]	Zr ₆ O ₄ (OH) ₄ (BDC) ₆ [68]	1290 [68]	1187 [125] 1030 [99]	0.49 [68] 0.52 [99]
	UiO-66-NH ₂	 [93]	N/A	N/A	905 [93]	N/A	0.43 [93]
	MOF-801-P	N/A	 [68]	Zr ₆ C ₂₄ H ₂₈ O ₃₈ Zr ₆ O ₄ (OH) ₄ (fumara te) ₆ [68]	990 [68]	1070 [68]	0.45 [68]
	MOF-801-SC	N/A	N/A	Zr ₆ C ₂₄ H ₂₈ O ₃₈ Zr ₆ O ₄ (OH) ₄ (fumara te) ₆ [68]	690 [68]	770 [68]	0.27 [68]

MOF-805	N/A	 [68]	$Zr_6O_4(OH)_4[NDC-(OH)_2]_6$ [68]	1230 [68]	1370 [68]	0.48 [68]
MOF-806	N/A	 [68]	$Zr_6O_4(OH)_4[BPDC-(OH)_2]_6$ [68]	2220 [68]	2390 [68]	0.85 [68]
MOF-812	N/A	 [68]	$Zr_6O_4(OH)_4(MTB)_3(H_2O)_2$ [68]	N/A	N/A	N/A
MOF-802	N/A	 [68]	$Zr_6O_4(OH)_4(PZDC)_5(HCOO)_2(H_2O)_2$ [68]	<20 [68]	<20 [68]	<0.01 [68]

MIL-53	Aluminium Fumarate MIL-53-Al	 [92]	 [50]	[Al(OH)(O ₂ C-CH CO ₂)] [92]	792.26 [66] 1021 [96]	1000-1200 [96]	0.926 [66] 0.48 [96]
	MIL-53-Ga	 [126]	 [127]	Ga(OH) _{0.9} (F) _{0.1} (BD C) _{0.9} H ₂ O [128]	N/A	N/A	N/A
CAU-13	CAU-13-Ga	 [126]	 [126]	N/A	N/A	N/A	N/A
MIL-100	MIL-100-Fe	N/A	 [97]	N/A	1917 [97]	N/A	1.00 [97]

MIL-100-Cr	N/A	 [98]	N/A	1130 [98]	N/A	0.77 [98]
Fe-BTC	 [55]	N/A	$C_9H_3FeO_6$ [55]	1300-1600 [55]	N/A	N/A

Key: N/A: not available; S_{BET} : specific BET surface area.

244

245

246 *2.2. Water-vapor adsorption equilibrium*

247 The MOFs usually exhibit continuous water-vapor adsorption uptake at all RH ranges due to
248 the macro, meso and micro pores' availability in their crystals. Water vapors were firstly settled
249 into macropores, followed by meso and micro pores. The MOFs usually exhibited various types
250 of water-vapor adsorption isotherms.

251 MOFs of the MIL series are extensively studied in the literature, which exhibited adsorption
252 isotherms of type-IV and type-V as per IUPAC classification. Water-vapor adsorption uptake of
253 Al-based MIL-53 (known as AIFs) was investigated in the literature [50]. Al and Ga metal-based
254 adsorbents were found to be more stable for water vapor adsorption due to Al and Ga metals' water
255 stability. MIL-53(Al) showed uptake of 0.36 kg/kg at relative pressure of 0.90 with adsorption
256 isotherm of type-IV [49,50,129]. Dubinin-Astakhov (D-A) based equations (Table 3) were used
257 depending upon the adsorption potential range to model the adsorption equilibrium data. The
258 adsorption uptake behaviour of MIL-53(Ga) was quite different from MIL-53(Al) due to the
259 presence of a large number of hydrated nano-pores in its crystals [130]. Moreover, iron (Fe) and
260 chromium (Cr) based MIL-53 have not shown good water vapour adsorption uptake [55]. The Cr
261 and Fe metal ions have shown more attraction for water-vapors than the organic linker and resulted
262 in adsorbents degradation. Chromium-based MIL-101 possessed an uptake of 1.45 kg/kg at
263 relative pressure of 0.90 [50]. It exhibited type-V adsorption isotherm, and D-A based equations
264 (depending upon relative pressure range) were used to fit adsorption equilibrium data as presented
265 in Table 3.

266 The adsorption properties can be improved by changing/adding functional groups/ coating
267 material with other hydrophilic metal(s) [94,131]. For example, the adsorption uptake of MIL-101
268 was improved to 1.60 kg/kg at a relative pressure of 0.90 when coated with GO to form MIL-
269 101(Cr)@GO [58,60,98]. Similarly, water-vapor adsorption uptake of MIL-100 was investigated
270 with aluminium and iron metals ions [132][96]. MIL-100(Fe) shown maximum uptake of water
271 vapors of 1000 cm³/g (at 273K) and exhibited type-V adsorption isotherm, which is relatively
272 higher (i.e. 0.70 kg/kg) as compared to MIL-100(Al) (i.e. 0.48 kg/kg) at 273K and relative pressure
273 of 0.90. MIL-100(Fe) had large hysteresis at the same temperature and relative pressures. It had
274 high hydrothermal stability as it is stable after 40 adsorption/desorption cycles and 5 hours per
275 cycle at the temperature range from 40 to 140 °C [97]. MIL-125 with functional group H₂N shown
276 uptake of 0.60 kg/kg (at a relative pressure of 0.9 and 273K) and owing to adsorption isotherm

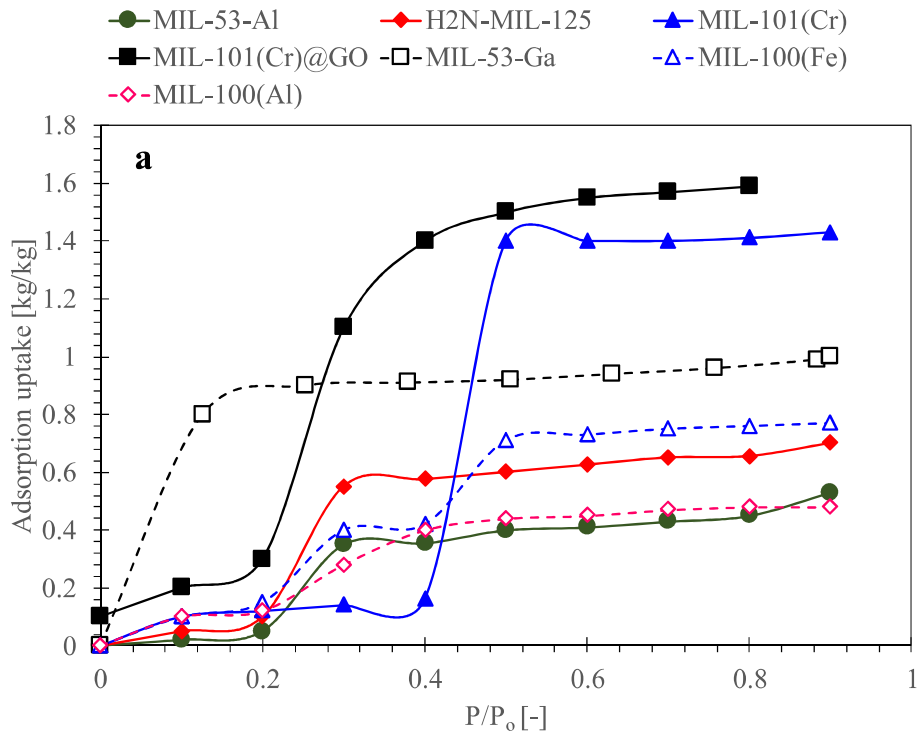
277 of type-IV [99]. A detailed comparison of water-vapor adsorption isotherms for MIL series-based
278 MOFs is provided in Fig. 4 (a). MIL-101 with Cr templet has shown the highest water-vapor
279 adsorption uptake than all other adsorbents of the MIL-series. A noticeable increase in the
280 adsorption uptake can be observed when MIL-101(Cr) was coated with Graphite oxide (GO) that
281 increased adsorption uptake ability and stability.

282 Similarly, Zr-based MOFs, e.g. MOF-801, MOF-805, MOF-806, MOF-802, MOF-841, MOF-
283 812 and MOF-808, were also investigated, which shown reasonable water-vapor adsorption uptake
284 [68,114]. Adsorption behavior of some Zr-based adsorbents was compared in a study [68] UiO-66
285 [115,117,119] with PIZOF-2 [113] and DUT-67 [119]. A detailed comparison of water-vapor
286 adsorption isotherms for Zr-series-based MOFs is provided in Fig. 4(b). UiO-66 shown water-
287 vapor uptake of $525 \text{ cm}^3/\text{g}$ at a relative pressure of 0.90 and temperature of 293K. However, UiO-
288 66 did not possess cyclic stability; hence, it was not suitable for cyclic use applications. On the
289 other hand, MOF-801 and MOF-841 exhibited good water-vapor adsorption uptake with cyclic
290 stability. These adsorbents could exhibit the same adsorption uptake for many cycles, and thereby
291 MOF-801 was found more promising adsorbent for cooling application [82].

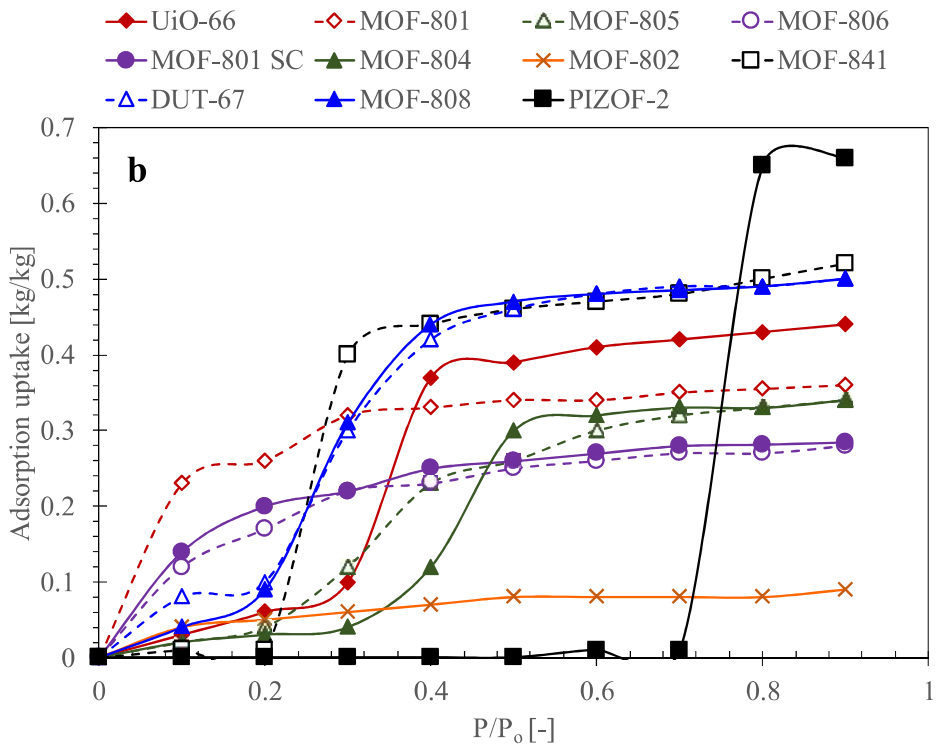
292 In addition to MIL and Zr-series, many other hydrophilic MOFs were investigated in the
293 literature, as summarized in Fig. 4(c). In a study [53], CPO-27 with nickel (Ni) metal node
294 possessed a high attraction for water-vapors. The D-A equation was used to fit the adsorption
295 equilibrium data [49,50,52,53]. The D-A model equations are provided in Table 2, whereas the
296 corresponding values for the optimized parameters are exhibited in Table 3.

297 Fig. 4(c) shows that type-I adsorption isotherm can be seen with maximum uptake of 0.45
298 kg/kg at a relative pressure of 0.90 and a temperature of 25°C . The CPO-27 possessed cyclic
299 stability for adsorption uptake even after 50 adsorption/desorption cycles [53]. Water-vapor
300 adsorption equilibrium for HKUST-1 and Fe-BTC has been experimentally investigated in the
301 literature [55]. Langmuir and Sip equations were used to model adsorption equilibrium data.
302 HKUST-1 showed type-1 adsorption isotherm and maximum uptake of 0.60 kg/kg at a relative
303 pressure of 0.90, thereby finding a more suitable adsorbent [37]. In another study [106], Dual-
304 Sided Langmuir-Freundlich (DSLFF) equation (Table 2) was used to fit water-vapor adsorption data
305 for HKUST-1. However, Fe-BTC showed type-III adsorption isotherm with a maximum uptake of
306 0.36 kg/kg at a relative pressure of 0.90. The optimized parameters for all models and all studied
307 adsorbents are provided in Table 3.

308



309

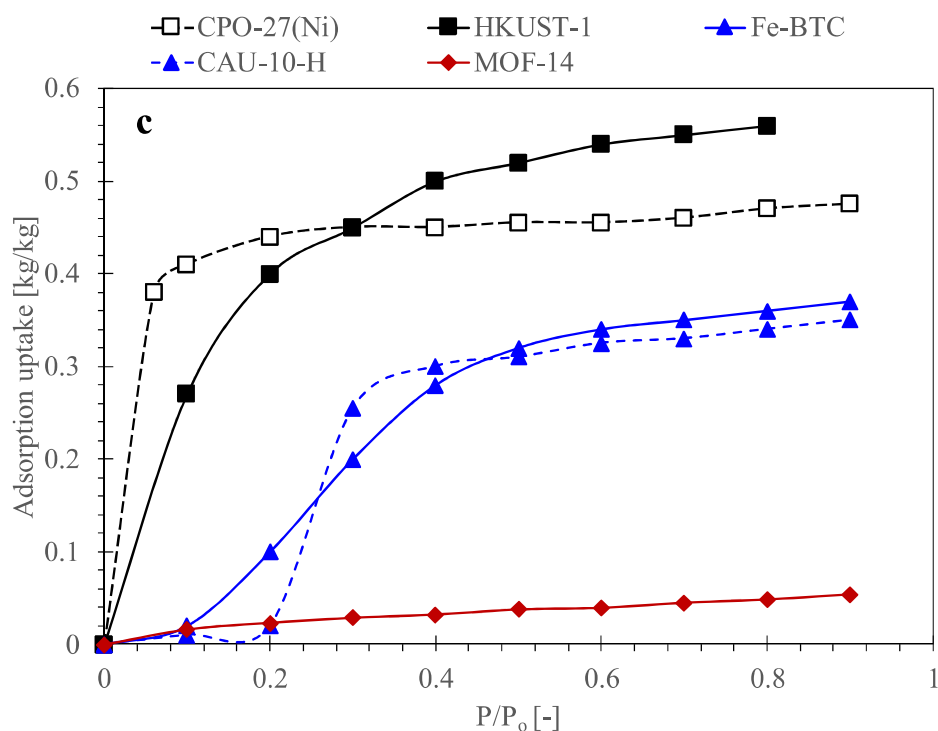


310

Fig. 4. Water-vapor adsorption isotherms for (a) MIL series-based MOFs, (b) zirconium-based

311

MOFs, and (c) other MOFs available in the literature.



312
 313 **Fig. 4.** Water-vapor adsorption isotherms for (a) MIL series-based MOFs, (b) zirconium-based
 314 MOFs, and (c) other MOFs available in the literature.

315
 316
 317 Some of the MOFs reported in literature did not show good water-vapor adsorption uptake e.g.
 318 Birm-1 [55], Birm-1-K [55], Birm-1-Li [55], MOF-5 [62] and MOF-14 [105]. However, they
 319 performed better for other applications like gas separation.

320
 321

322 **Table 2.** Fundamental equations of the adsorption equilibrium models used in the literature for fitting of adsorption isotherms data of
 323 various MOF/water pairs.

Adsorption equilibrium model	Governing equation(s) of the model	MOFs
D-A equation	$w = w^{\circ} \exp\left(-\left(\frac{A}{E}\right)^n\right)$ $A = R T \ln\left(\frac{P}{P_0}\right)$	CPO-27 (Ni) [49,50,53] MIL-101(Cr) [50] Aluminum fumarate [50]
Dual-site Langmuir-Freundlich equation	$w = w_{m1} \frac{b_{DSL1} P^{1/n_{DSL1}}}{1 + b_{DSL1} P^{1/n_{DSL1}}} + w_{m2} \frac{b_{DSL2} P^{1/n_{DSL2}}}{1 + b_{DSL2} P^{1/n_{DSL2}}}$	HKUST-1 [106]
Langmuir equation	$w = \left[w^{\circ} \left[b \cdot \left(\frac{P_{sat,T_{ref}}}{P_{sat,T_{abs}}} \right) \left(1 + b \cdot \left(\frac{P_{sat,T_{ref}}}{P_{sat,T_{abs}}} \right) \right) \right] \right]$ $w = w^{\circ} \frac{b \left(\frac{P}{P_0} \right)}{1 + b \left(\frac{P}{P_0} \right)}$	HKUST-1 [55]
Freundlich equation	$w = H \left(\frac{P}{P_0} \right)^{1/m}$	MIL-101 (GO) [60]
Sip equation	$w = w^{\circ} \frac{b \left(\frac{P}{P_0} \right)^{1/n}}{1 + b \left(\frac{P}{P_0} \right)^{1/n}}$	MIL-101 (GO) [60] Fe-BTC [55]

324

325

326 **Table 3.** Optimized fitting parameters of the adsorption equilibrium models used in the literature for fitting of adsorption isotherms data
 327 of various MOF/water pairs.

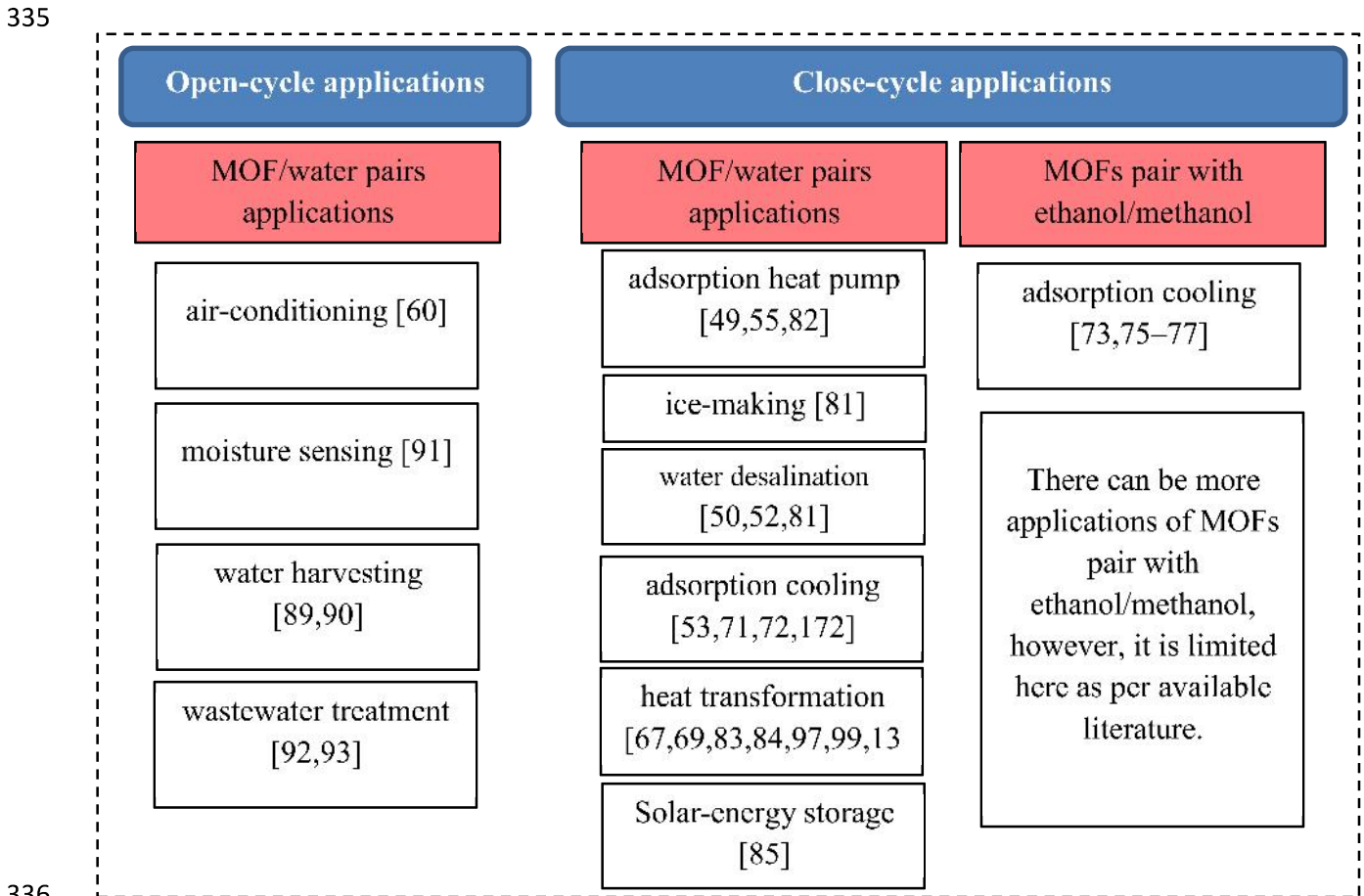
Adsorption equilibrium model	MOFs	Optimized parameters of the models	Temperature [°C]	References					
D-A equation	CPO-27 (Ni)	$n=4$ $E=10014\text{J/mol}$ $w^{\circ}=0.462\text{kg/kg}$	25	[49] [52]					
	MIL-101 (Cr)	$w = 0.42434 \exp(-0.0002825A)$ for $\frac{P}{P_0} \leq 0.15$ $w = 0.4636 - 0.00024A + 5.4E - 08A^2 - 4.06E - 12A^3$ for $0.15 < \frac{P}{P_0} \leq 0.4$ $w = 1.51 - \left(\frac{A}{1.35^*T}\right)$ for $0.4 < \frac{P}{P_0} \leq 0.5$ $w = 1.51 - 0.000266A + 0.363E - 6A^2 - 0.177E - 9A^3$ for $\frac{P}{P_0} > 0.5$	15-45	[50]					
Freundlich equation	Aluminum Fumarate	$w = 0.111993 \exp(-0.000258797A)$ for $A > 3987$ $w = 2.36129 - 9.93768E - 04A + 1.05709E - 07A^2$ for $2900 \leq A \leq 3987$ $w = -3.124455E - 11A^3 + 1.68302E - 07A^2 - 3.12E - 04A + 0.5948$ for $A < 2900$	25	[50]					
	MIL-101 GO	$H=0.59 \text{ kg/kg}$; $m=1.2$ for $\left(\frac{P}{P_0} \leq 0.35\right)$	25	[60]					
Dual site Langmuir-Freundlich Equation	HKUST-1	Temperature (K)	w_{m1} (mmol/g)	b_{DLSLF1} (mbar ^{1/n})	w_{m2} (mmol/g)	b_{DLSLF2} (mbar ^{1/n})	$1/n_{\text{DLSLF}}$	[106]	
		288	22.54	0.385	0.656	10.63	1.037×10^{-14}		0.0813
		298	20.77	0.11	0.569	11.51	0.102×10^{-17}		0.0849
		308	17.38	0.0253	0.478	13.82	2.015×10^{-14}		0.1202
		318	14.65	0.0045	0.428	16.52	2.658×10^{-18}	-.1635	
Sip equation	Fe-BTC	$w^{\circ}=0.38 \text{ kg/kg}$ $b=2.75$ $n=3.63$	52	[55]					

	MIL-101 GO	$w^o=1.55 \text{ kg/kg}$ $b=4.48 \times 10^3$ $n=0.0847$ for $\frac{P}{P_o} \geq 0.35$	25	[60]
Langmuir equation	HKUST-1	$w^o=0.64 \text{ kg/kg}$ $b=8.33$	52	[55]

328

329 **3. Applications of MOF/water pairs**

330 In recent decade, the MOFs adsorbents are extensively investigated for the development of
 331 open and close-cycle adsorption applications. Water is a typical adsorbate in case of open-cycle
 332 system application [60,89,91–93,133], whereas, ethanol [75–77], methanol [73] and water
 333 [49,50,52,53,55,67,72,81,83,97,99,134] are studied for closed-cycle system applications. Detail of
 334 applications is summarized in Fig. 5.



337 **Fig. 5.** Insights of applications of MOF adsorbents studied in the literature.

338

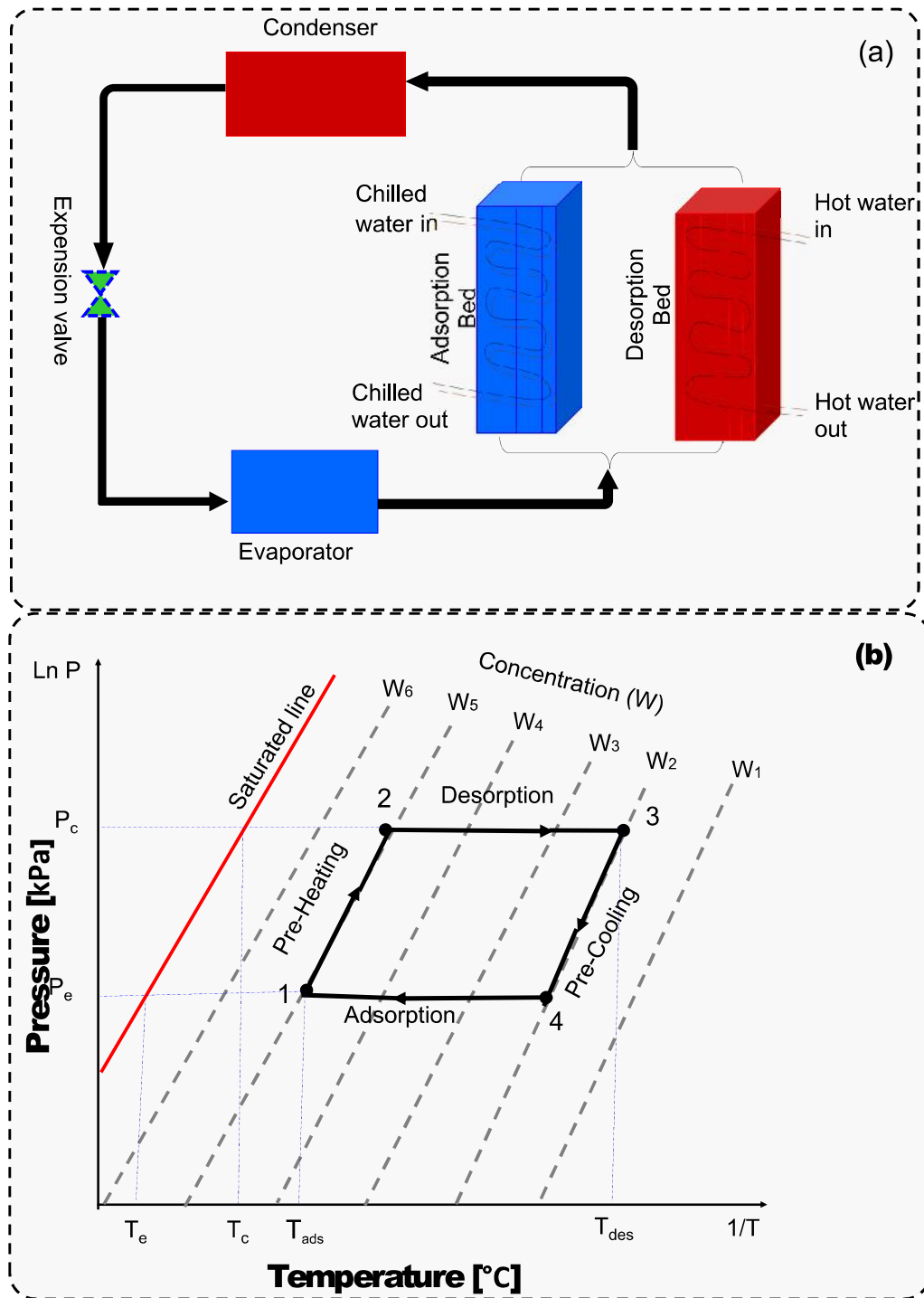
339 *3.1. Adsorption cooling*

340 Adsorption cooling systems are mainly closed-cycle systems consisted of an evaporator,
 341 adsorption beds, expansion valve, condenser, and associated accessories. Fig. 6 (a,b) shows a
 342 typical schematic diagram of a closed-cycle adsorption cooling system and a Pressure-
 343 Temperature-Concentration (P-T-W) diagram demonstrating the ideal thermodynamic cooling
 344 cycle. Various adsorption cooling technologies/systems based on different cooling cycles have

345 been reported in the literature [135–142]. It has been found that the COP and SCP of the system
346 are mainly affected by heating sources [143,144], adsorption equilibrium and adsorbent-adsorbate
347 interaction [3,145–147]. In this regard, MOFs are investigated with various adsorbates, e.g. water
348 [148], ethanol [149] and methanol for adsorption cooling applications. The MOFs showed high
349 adsorption uptake, even at lower concentrations [150]. For example, MIL-101(Cr) shown
350 maximum uptake of ethanol, methanol and water of 1.10 kg/kg [77], 1.20 kg/kg [73] and 1.45
351 kg/kg [49], respectively. The MIL-101(Cr)/ethanol pair has been experimentally investigated in
352 literature for adsorption cooling [77] and refrigeration [75] applications. MIL-101(Cr) possessed
353 a methanol uptake of 0.51 kg/kg, which is twice that of activated carbon (i.e. 0.234 kg/kg).
354 Adsorption equilibrium and kinetics have been experimentally tested, and the results revealed, it
355 could be a promising candidate for developing cooling devices [77]. In a study [75], MIL-101(Cr)
356 showed adsorption ability for many adsorption-desorption cycles (stable after 60 cycles) as the
357 reduction in BET surface area was only 3.30%. MIL-101(Cr)/ethanol is completely regenerated at
358 100°C, a relatively low regeneration temperature than activated carbons. Similarly, MIL-101(Cr)
359 and HKUST-1 were investigated for methanol adsorption uptake [73]. The results showed that
360 MIL-101(Cr) has higher performance when desorption temperature is less than 353K. However,
361 HKUST-1 has higher performance when evaporator temperature is greater than -5°C and
362 outperformed compared to activated carbons.

363 Hydrophilic MOFs have been investigated in the literature for single and two beds adsorption-
364 based air-conditioning and cooling systems. In a study [53], CPO-27(Ni) has been experimentally
365 tested to develop a single-bed adsorption refrigeration system and simulated for two beds
366 adsorption systems for automobile air-conditioning. This study also compared the performance of
367 CPO-27(Ni), RD-2060 and SAPO-34 to select appropriate adsorbent with higher COP and SCP
368 values. Results have shown that CPO-27(Ni) has good performance with SCP values ranging from
369 80 W/kg to 105 W/kg. However, SAPO-34 outperformed both cases with the SCP value of
370 440W/kg and a regeneration temperature of 130°C, which is quite higher than CPO-27(Ni). There
371 is an effect of condenser and evaporator temperature on SCP and COP of the system. In a study
372 [49], CPO-27(Ni) was investigated for adsorption heat pump applications where it was best
373 operated at low evaporator temperature (< 5°C). Similarly, HKUST-1 and seven more MOFs [55]
374 were investigated for adsorption chiller applications. The results showed that HKUST-1 has higher

375 performance at lower evaporator temperature ($< 5^{\circ}\text{C}$) and 185% more water-vapor uptake than
 376 silica-gel.



377
 378 **Fig. 6.** (a) Schematic diagram of the adsorption cooling system, and (b) P-T-W diagram of the
 379 adsorption cooling cycle.

380 However, not all the MOFs need to require low evaporator temperature for good performance,
 381 e.g. AIFs requires a high evaporator temperature of 20°C [49]. In the case of the adsorption heat
 382 pump, the useful energy is heat used by the evaporator, condenser and adsorption beds/wheel.
 383 COP_h can be calculated by Equation 1 [49].

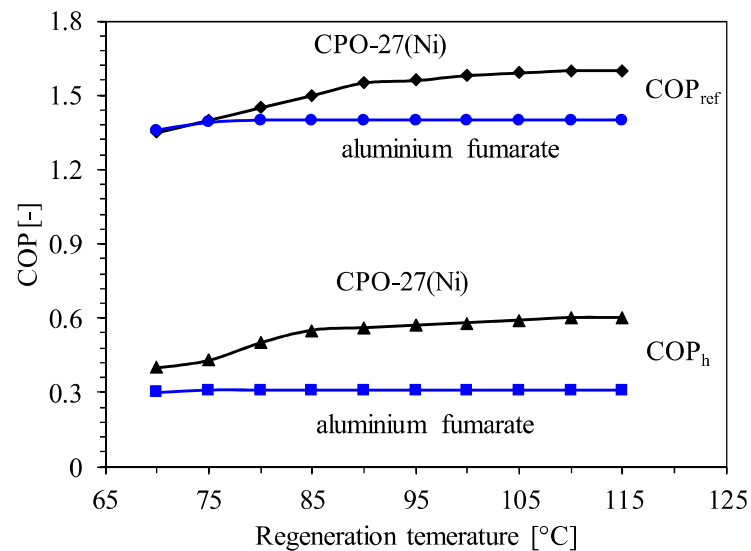
$$384 \text{ COP}_h = \frac{Q_{ads} + Q_c}{Q_{des}} \quad (1)$$

385 For an adsorption chiller, the evaporator energy is the useful energy from the device. COP_{ref} is
 386 calculated by Equation 2.

$$387 \text{ COP}_{ref} = \frac{Q_e}{Q_{des}} \quad (2)$$

388 The effect of regeneration temperature for CPO-27(Ni) and aluminium fumarate is shown in
 389 Fig. 7. It can be observed that COP_h and COP_{ref} of aluminium fumarate remain constant after 75°C.
 390 However, in the case of CPO-27(Ni), it continuously increases up to 90°C then becomes constant
 391 up to 115°C. In another study [71], MIL-125-H₂N finds a promising candidate with SCP values
 392 ranging from 0.4-2.8 kW/kg with high cyclic and hydrothermal stability and low regeneration
 393 temperature. The feasibility of different hydrophilic MOFs and their use for closed-cycle
 394 applications is given in Table 4.

395



396 **Fig. 7.** Effect of regeneration temperature on COP at T_{con}=35°C and T_{eva}=5°C reproduced from
 397 [49].
 398

399 **Table 4.** Applications of the hydrophilic MOFs considered in the literature using close-cycle systems.

MOFs	Methodology used	Application(s)	Regeneration temperature [°C]	Condenser temperature [°C]	Evaporator temperature [°C]	Findings and conclusion	Reference
CPO-27(Ni)	Modeling	Adsorption heat pumps	≥90	30-45	5	<ul style="list-style-type: none"> • High temperature regeneration greater than 90°C • Low evaporator temperature 	[49]
	Dynamic modeling + experiment + Simulation	Automotive air-conditioning	≥90 and up to 130	15-35	5-25	<ul style="list-style-type: none"> • Single and two-beds air-conditioning system and COP value is 0.3 • SCP= 80-105 W/kg • Two beds adsorption cooling system has cooling capacity and SCP values of 2.4 kW and 400 W/kg, respectively, at cycle time of 900 seconds and desorption temperature of 130°C 	[53]
Aluminum fumarate	Modeling	Adsorption heat pump	70	40-45	20	<ul style="list-style-type: none"> • Suitable for Low regeneration temperature less than or equal to 70°C • High evaporator temperature greater than 20°C 	[49]
NH ₂ -MIL-125	Experiment + dynamic modeling	Adsorptive cooling	90	N/A	N/A	<ul style="list-style-type: none"> • Suitable for High COP at low desorption/regeneration temperature • SCP=0.4-2.8 kW/kg • High hydrothermal stability 	[71]
HKUST-1	Experiment + analysis	Adsorption chiller	85	32	5	<ul style="list-style-type: none"> • Suitable for More uptake 185.7 % compared to silica-gel at evaporator temperature 5°C • Low evaporator temperature of 5°C 	[55]

Triazolyl phosphonate MOF	Modeling/ simulation	Adsorptive cooling	110	N/A	N/A	Suitable for <ul style="list-style-type: none"> Regeneration temperature higher than 110°C is not meaningful so operating on low temperature. Higher performance than zeolite 	[72]
Fe-BTC	Experiment	Adsorption chiller	85	32	12	Suitable for <ul style="list-style-type: none"> Cascade cooling High performance at high evaporator temperature greater than 10°C 	[55]
MOF-801	Experiment	Adsorption cooling	80-85	30	5	<ul style="list-style-type: none"> High performance with COP is 0.67 and SCP is 0.29±0.01 Kw/kg Isosteric heat of adsorption 55 to 60 kJ/mol in the uptake range 0.05–0.35 kg/kg 	[82]
MIL-100(Fe)	Experiment	Adsorption cooling	95	20	N/A	Suitable for <ul style="list-style-type: none"> Energy storage density is 1200 Wh/kg and COP is 0.8 with cycle time of 90 mint It produced cooling effect of 337 W/kg 	[129]

400 **Key:** N/A: not available

401

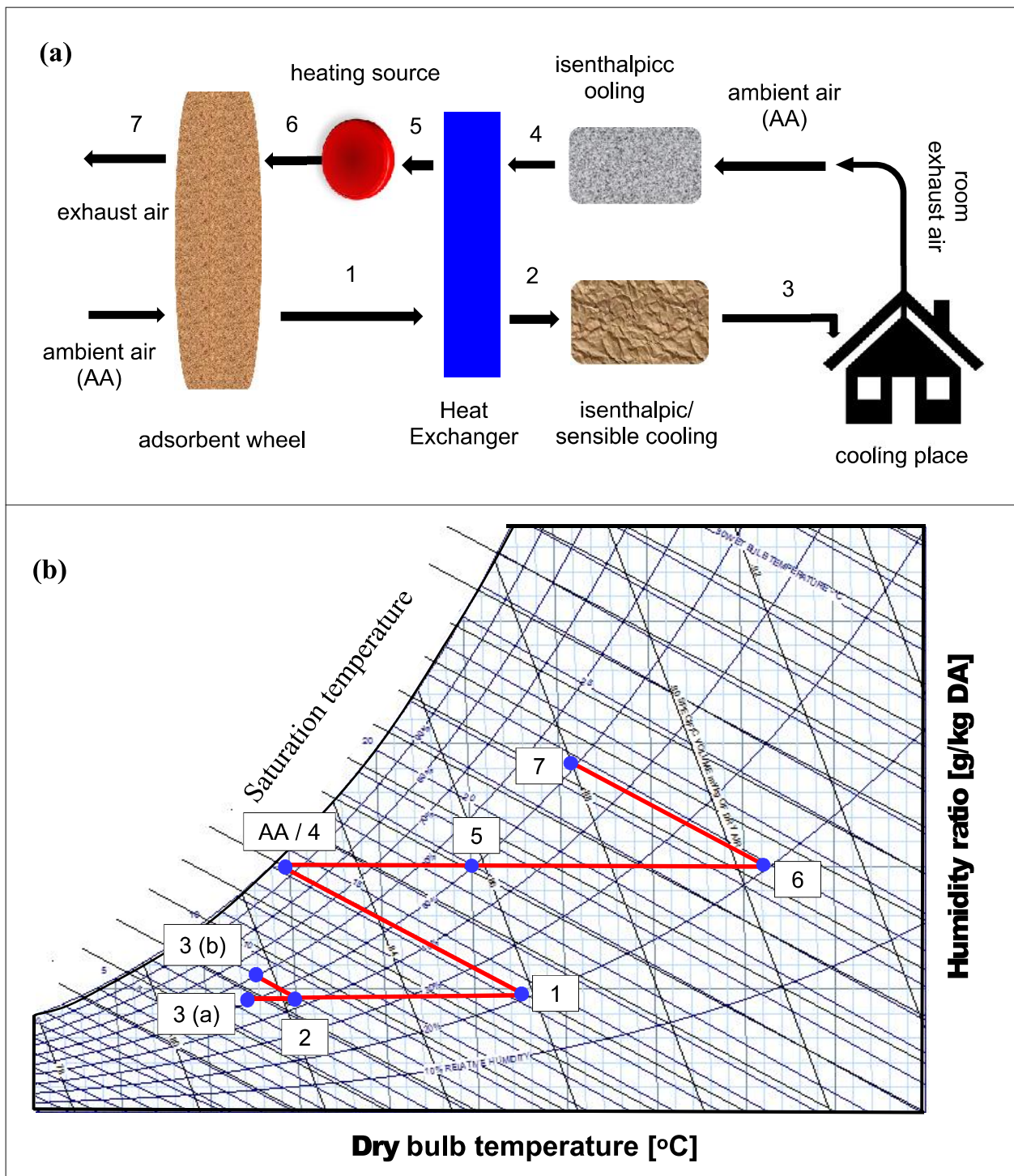
402 3.2. Desiccant air-conditioning

403 The desiccant air-conditioning (DAC) system usually consists of a desiccant unit (wheel/rotor
404 or block type), heat exchanger, heating source, a low-cost cooling source, and some associated
405 accessories [151]. A typical schematic diagram of a DAC system and the corresponding
406 psychrometric representation of the DAC cycle are shown in Fig. 8(a) and (b). In a study [60],
407 MIL-101(Cr)@GO has simulated for adsorption air-conditioning open-cycle system and results
408 were compared with conventionally used silica-gel based system. Different parameters were
409 investigated, e.g. rotational speed, cooling energy consumption, thermal energy consumption,
410 energy, environmental and economic analysis and dehumidification efficiency of the desiccant
411 wheel (DW). Dehumidification effectiveness (DE) is calculated by Equation 3 [60].

412
$$\eta_{\text{deh}} = \frac{w_{\text{pro,in}} - w_{\text{pro,out}}}{w_{\text{pro,in}}} = 1 - \frac{w_{\text{pro,out}}}{w_{\text{pro,in}}} \quad (3)$$

413 Dehumidification effectiveness was taken as a function of the process air RH.
414 Dehumidification effectiveness increases when temperature and RH of inlet air increases, as shown
415 in Fig. 9. The DE of MIL-101(Cr) is higher than silica-gel; this is because of the high uptake of
416 MIL-101(Cr).

417 In another study [152], a solar-driven HKUST-1 based DAC system was simulated. A
418 comparison between silica-gel (type B) coated heat exchanger (SCHE), and MOFs coated heat
419 exchanger (MCHE) at different outlet temperatures had made. The MCHE has 1.28 times more
420 dehumidification capacity than SCHE when cycle time 120s, as shown in Fig. 10. The
421 dehumidification capacity of MCHE rises with an increase in regeneration temperature at a cooling
422 water temperature range of 25°C and 30°C. In SCHE, the increase in dehumidification capacity is
423 very low, with an increase in regeneration temperature. MCHE was found to be more applicable
424 for a shorter cycle time than SCHE due to the low water holding capacity of HKUST-1.

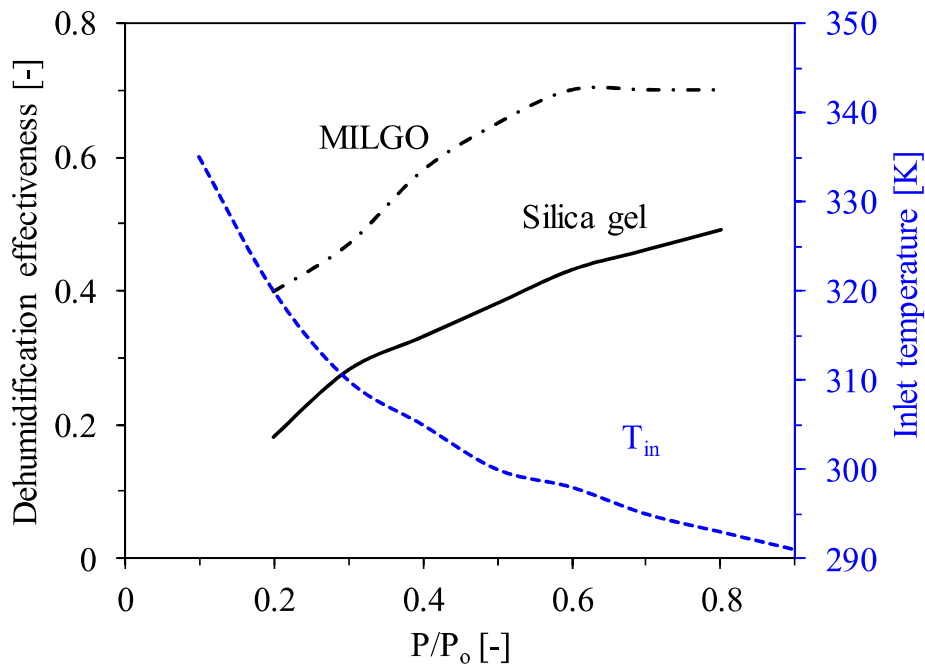


425

426

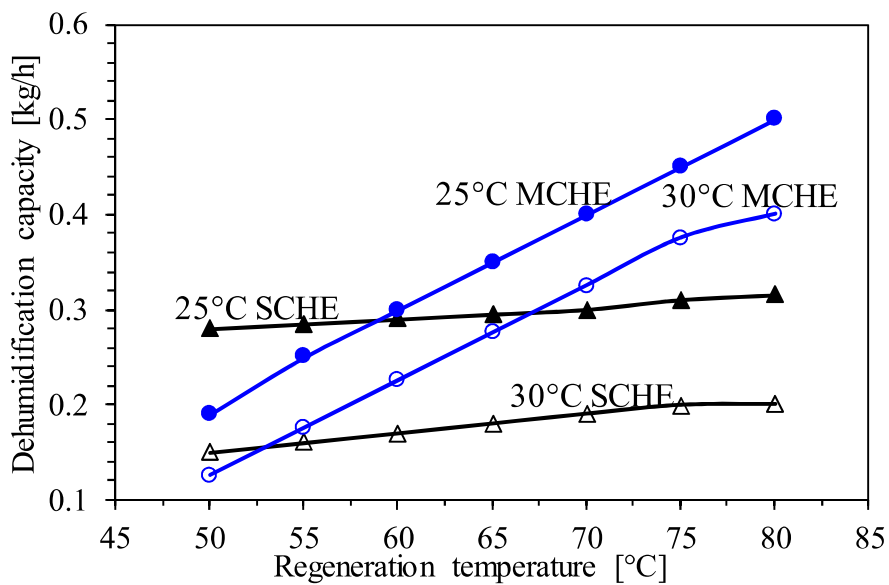
427

Fig. 8. (a) Schematic diagram of the desiccant air-conditioning system and (b) Psychrometric representation of the desiccant air-conditioning cycle.



428

429 **Fig. 9.** Comparison of dehumidification effectiveness by silica-gel as a function of relative
 430 pressure of process air of MOF based adsorbents (for process absolute air humidity of 0.01 kg/kg
 431 and desorption temperature of 333K [60].



432

433 **Fig. 10.** Dehumidification capacity of MCHE and SCHE systems at cooling water
 434 temperatures of 25°C and 30°C [152].

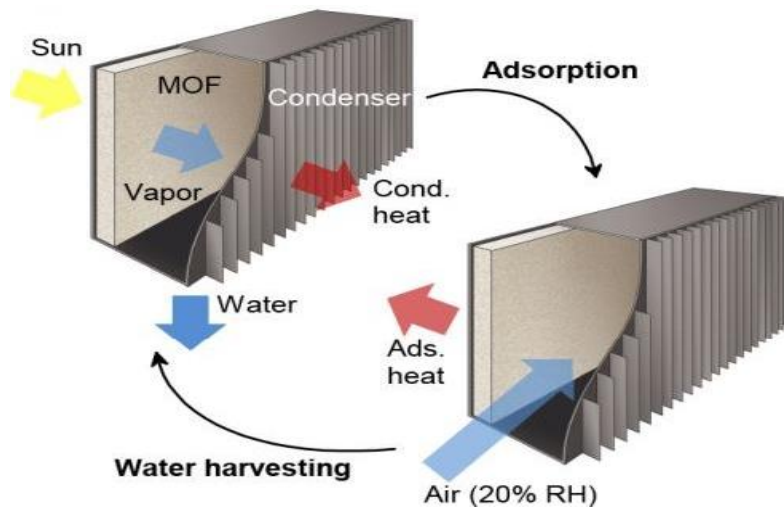
435

436 3.3. *Water harvesting and desalination*

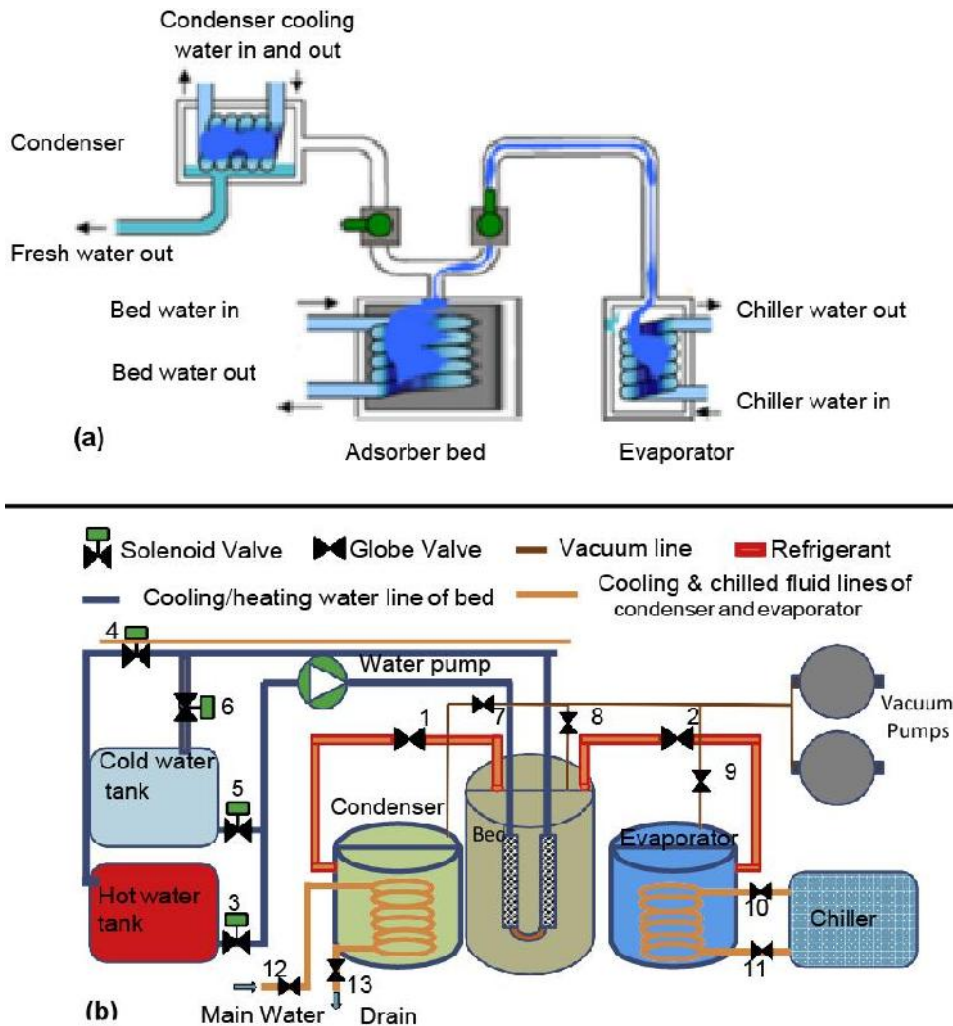
437 Water harvesting can be a promising application of the MOFs as they can adsorb water at low
438 concentration, and desorption occurs at relatively low temperature [133]. A Zr-based water
439 harvesting device for arid climate has been designed and investigated in a study, as shown in Fig.
440 11 [89]. It is estimated that currently, 150 countries are producing desalination water of about 30
441 billion m³/year by operating 18000 desalination plants [153,154]. Many studies have been reported
442 in the literature in which silica-gel and other conventional adsorbent have successfully investigated
443 for single-/ two-bed adsorption desalination systems [155–166]. However, the MOFs have been
444 utilized for water desalination application and freshwater production, ice and some amount of
445 cooling. In another study [52], CPO-27(Ni) has experientially investigated water desalination for
446 a one-bed adsorption-based desalination system. A schematic diagram of the single bed of
447 adsorption-based desalination system is shown in Fig. 12. The performance of the water
448 desalination system is assessed on the specific daily water production (SDWP), which can be
449 calculated by using Equation 4 [52].

450
$$SDWP = \int_0^{t_{\text{cycle}}} \frac{Q_{\text{cond}} \cdot \tau}{h_{fg} M_a} dt \quad (4)$$

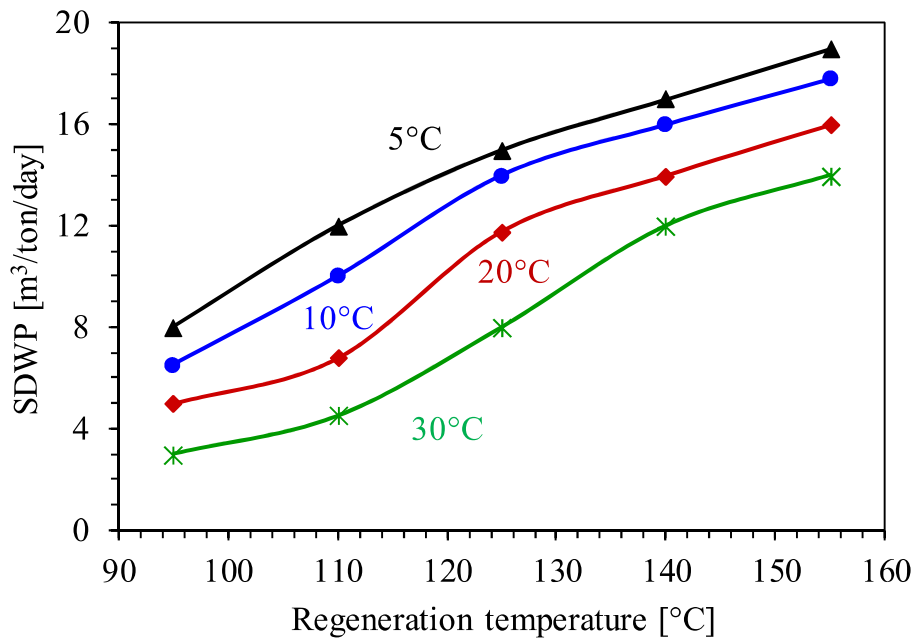
451 The SDWP of the system was affected by desorption and the condenser temperature, the effect
452 of regeneration temperature on the SDWP is shown in Fig. 13. SDWP at different condenser and
453 regeneration temperature reproduced from [52]. It can be observed that most of the MOFs shown
454 good results when operated at low condenser temperature, e.g. CPO-27(Ni) has maximum water
455 production of 22.8m³/tone. ads/day and producing cooling of 219.9 Rton/tonne when operated at
456 maximum inlet condenser temperature of 5°C and inlet evaporator temperature of 40°C. Therefore,
457 reducing the condenser temperature and increasing the evaporator temperature results in maximum
458 water production and increased cooling capacity. In another study [50], three MOFs, CPO-27(Ni),
459 MIL-101(Cr) and aluminium fumarate (AIFs) have investigated for two beds adsorption-based
460 desalination systems. CPO-27(Ni) gave maximum water production at low condenser temperature
461 and high evaporator temperature with a regeneration temperature of ≥110°C. Similarly, AIFs
462 performed better at a high evaporator temperature of 20°C with water production of 6.3 m³/ton.day.
463 However, it required a low regeneration temperature of 70°C. In this regard, MIL-101(Cr)
464 performed good and shown exceptional results with maximum water production of 11 m³/ton.day.



465
466 **Fig. 11.** MOF based water harvesting device driven by natural sunlight [89].



467
468 **Fig. 12.** Schematic diagram of (a) single bed water desalination system [52] and (b) one be
469 adsorption based water desalination and ice-making system [81].



470
471 **Fig. 13.** SDWP at different condenser and regeneration temperature reproduced from [52].
472

473 CPO-27(Ni) is the best candidate for adsorption-based desalination system because of its shape
474 of adsorption isotherm and maintains its adsorption capacity when the relative pressure ratio is
475 maintaining. In another study [81], water desalination systems combined with ice-making with
476 one-bed adsorption system have been experimentally investigated. A schematic diagram of water
477 desalination combined with an ice-making system is shown in Fig. 12(b). CPO-27(Ni) used to
478 obtain maximum water and ice production is 1.8 ton/day/ton-ads and 8.3 ton/day/ton-ads,
479 respectively, to achieve a low evaporator temperature of 5°C. The applicability of different
480 hydrophilic MOFs for various applications is given in Table 5.
481

Table 5. Applications of the hydrophilic MOFs considered in the literature using open-cycle systems.

MOFs	Methodology used	Application(s)	Regeneration temperature [°C]	Condenser temperature [°C]	Evaporator temperature [°C]	References
OPEN-CYCLE SYSTEMS						
MIL-101(Cr)@GO	Simulation + case study	Air-conditioning	50-70	N/A	N/A	[60]
	<u>Findings and conclusion</u> <ul style="list-style-type: none"> The dehumidification efficiency of MIL-101(Cr)@GO is higher than silica-gel The rotational speed of MIL-101(Cr)@GO is significantly higher than silica-gel as high water-vapor uptake the optimal speed is 40 rev/h Thermal energy consumption for the regeneration of DW is 40 % lower than silica-gel, resulting in a reduction in cooling energy consumption about 11 % than silica-gel Energy, environment and economic analysis showed that MIL-101(Cr)@GO based DW has significant improvements than silica-gel based DW 					
HKUST-1	Simulation	Desiccant cooling	80	N/A	N/A	[152]
	<u>Findings and conclusion</u> <ul style="list-style-type: none"> Dehumidification capacity of MCHE is 1.28 times higher than SCHE when cycle time 120s The dehumidification capacity of MCHE is higher than SCHE when cycle time is shorter and cooling water temperature is high approximately equal to 80°C for long time period more than 240s SCHE performance is good as compare to MCHE HKUST-1 has good performance when cycle time is 120s and cooling water temperature is 80°C 					
PHCM-MOF	Simulation	Humidity control	≥40	N/A	N/A	[86]
	<u>Findings and conclusion</u> <ul style="list-style-type: none"> Maximum water-vapor adsorption uptake of 1.63 kg/kg at RH of 80 % and temperature of 25°C with S shape of adsorption isotherm Adsorption occurs when RH is higher than 40 % and desorption start when RH reduce to 45 % 					
WATER HARVESTING AND DESALINATION SYSTEMS						
MOF-801	Experiment	Water harvesting	≥85	33	N/A	[89,133]
	<u>Findings and conclusions</u> <ul style="list-style-type: none"> The total amount of harvested water is predicted at the end of all adsorption and desorption cycles in a day. It can harvest water about 0.19 L/kg of MOF after overcoming all kinetics limitations. Predicted water harvesting ability which is 0.28 L/kg at condenser temperature of 33°C and absorber temperature of 100°C Experimental water production is 0.21 L of water per kg of MOF at RH 40 % for a single cycle which is nearly same as predicted water production Harvested water has good quality as MOF-801 has higher hydrothermal stability and zirconium metal is stable in presence of water 					

<ul style="list-style-type: none"> MOF-801 is a promising candidate to work at low RH ranging from 15-20% at regeneration temperature is high 85°C MOF-801 has capacity to harvest water 2.8L/kg of MOF daily at RH as low as 20 % and no input of energy required 					[50,52,81]
CPO-27(Ni)	Experiment + numerical modeling, Experiment + simulation	Water desalination+ ice-making, water desalination cooling	≥110	40	5
<u>Findings and conclusion</u> <ul style="list-style-type: none"> Sea water and fresh water used as refrigerant to achieve low evaporator temperature $\leq 0^{\circ}\text{C}$ Production of ice= 8.3ton/day/ton-ads, COP of 0.9 and desalination of water of 1.8ton/day/ton-ads with optimum salinity is 35,000 ppm Produce 5.4 times more SDWP with value of 8.9 ton/day/ton-ads using sea and fresh water as refrigerant as compare to ammonia used in conventional systems Maximum water production= 22.8 m³/tonne.ads/day, cooling=215.99 Rton/tonne with condenser inlet temperature= 40°C and evaporator inlet temperature= 5°C 					
Aluminum fumarate	Modeling	Water desalination	70-85	25	20
<u>Findings and conclusions</u> <ul style="list-style-type: none"> It has SDWP and SCP of 6.30 m³/ton.day and 21.2 Rton/tonne, respectively In another study it has maximum SDWP 25.5 m³/ton.day and SCP of 789.4 W/kg 					
MIL-101 (Cr)	Modeling	Water desalination	N/A	N/A	N/A
<u>Findings and conclusions</u> <ul style="list-style-type: none"> Outperform with maximum SDWP of 11m³/ton.day 					
MIL-100(Fe)	Experimental + modeling	Water desalination	95	20	N/A
<u>Findings and conclusions</u> <ul style="list-style-type: none"> Maximum SDWP is 14 m³/ton.day with moderate cooling effect, and without cooling effect its SDWP is 19 m³/ton.day at high evaporator temperature 					

483

Key: N/A: not available

484

4. Prospects of MOFs adsorption systems and barrier in the commercialization

Although the adsorption phenomenon is well-known for centuries, however, considering this conception for cooling, air-conditioning and water desalination applications is started in the twentieth century to replace environmentally harmful compressor-based systems. From that moment, researchers worldwide are working to develop energy-efficient adsorption-based technologies/systems. In this regard, their research's key focus is to develop optimum adsorbent materials by which the overall efficiency/performance of the adsorption systems can be improved. The optimum material should have the ability to adsorb a larger amount of adsorbate for a wide range of system applications. The MOFs are a new class of micro- and nano-porous group of adsorbents with exclusive adsorption and physical properties. Recently, MOFs have been extensively investigated for the development of such systems. Fig. 14 shows a comparison between the studied five groups of hydrophilic MOFs. It was found that MIL series-based MOF have greater potential in various water adsorption and air-conditioning applications due to their stable structure and higher adsorption uptake. On the other hand, Cu-based MOFs perform better at relatively low-pressure and are highly dependent on pressure changes. Besides, Cu-Cu bond length elongates in the presence of moisture, increasing the moisture stability of this group in lower pressure ranges.

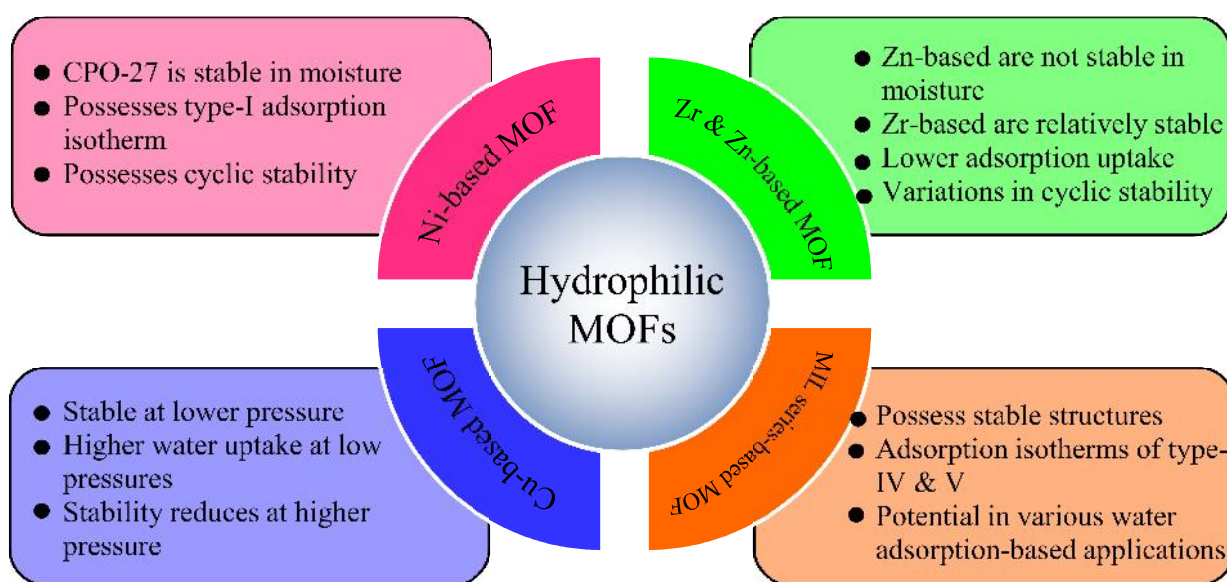
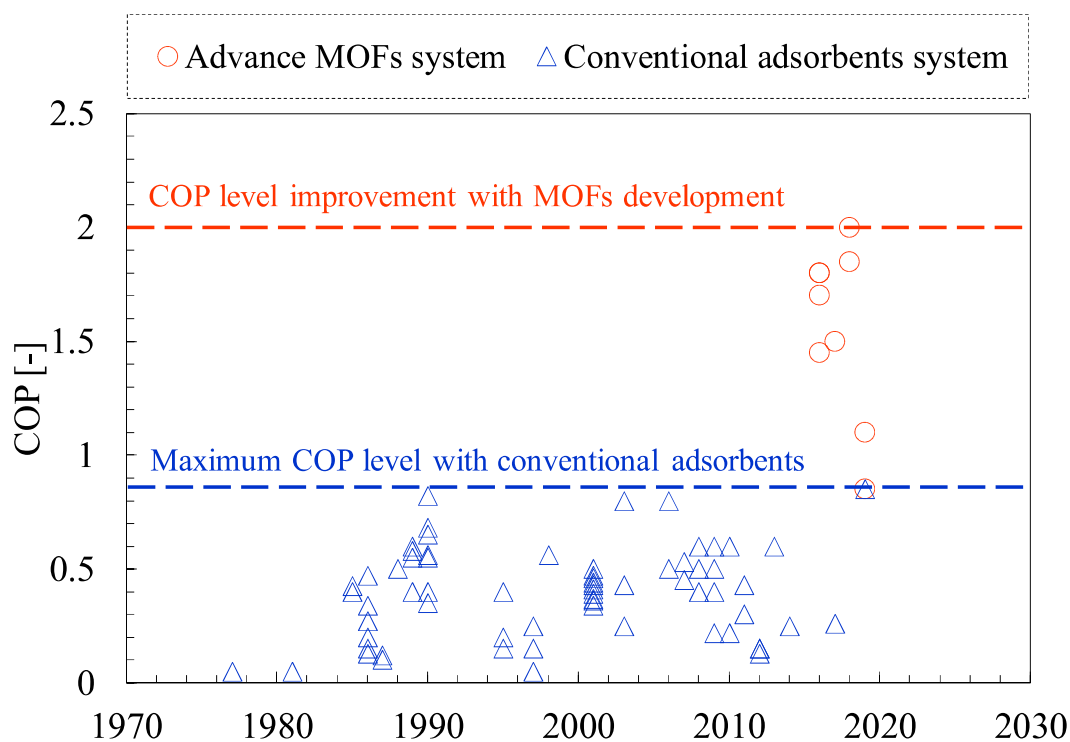


Fig. 14. A comparison of adsorption characteristics between the studied groups of hydrophilic MOFs, i.e. Ni-based, Cu-based, Zr-based, Zn-based and MIL series-based MOFs.

505 A state-of-the-art comparison of COP between the MOFs and conventional adsorbents-based
506 cooling systems is developed in Fig. 15 from 1975 to 2020. The adsorbents used for this
507 comparison are referred from following studies [8,10,17–
508 19,27,28,34,37,41,49,70,74,78,87,88,129,135–144,147–151,157,158,168–170]. The conventional
509 adsorbents-based systems are only able to achieve a COP level of 0.85 since 1975. However, the
510 majority of the MOFs based systems provide considerably higher performance as compared to
511 conventional adsorbent based systems. The main bottleneck in the lower COP level is the low
512 adsorption equilibrium amount. It has been found that conventional adsorbents possess low water-
513 vapor uptake, which results in low system performance and high system size. The MOFs exhibit
514 2 to 3 times higher water-vapor adsorption uptake as compare to conventional silica-gel. Some of
515 the MOFs result in adsorption uptake of 1.45 kg/kg, which can be increased to 1.60 kg/kg by
516 coating techniques. Therefore, this review is aimed to provide comprehensive detail of water-vapor
517 adsorption uptake by the hydrophilic MOF adsorbents available in the literature. The development
518 of high adsorbate uptake MOF materials helps to overcome the limitations of conventional
519 adsorbent systems, and the COP level is improved to almost 2. Similarly, the dehumidification
520 capacity of the MOF coated heat exchanger is found 1.28 times higher compared to the silica-gel
521 coated heat exchanger. The MOFs produce maximum desalination water of 25.5 m³/ton.day, which
522 is higher than silica-gel (i.e. 13.5 m³/ton.day). The energy consumption and
523 environmental/economic analyses conducted in the literature show that the MOF systems are a
524 better option than conventional systems.

525 Based on crystal, structural properties and water-vapor adsorption equilibrium amount, it can
526 be summarized that the development of advance MOFs is strengthening the desperate attempts to
527 develop energy-efficient and high-performance adsorption systems. The MOF adsorption systems
528 are coming strongly to the commercial market and we may soon see one of these systems sold
529 commercially. However, a lots of future works are needed to commercialize them accordingly and
530 to replace the traditional technologies. Considering the above-mentioned prospectus of the MOF
531 adsorbents/systems, the recommended future works include: (i) Developing the optimum MOF
532 adsorbents with sophisticated thermo-physical properties including pore volume, surface area,
533 thermal conductivity, and crystal structure etc. (ii) Characterizing, measurement and treatments of
534 adsorbent-adsorbate pairs for the development of advance adsorption capacities (including
535 adsorption equilibrium, adsorption kinetics, and adsorption heat) for various heat transformation

536 applications, (iii) Integration of advance MOFs in adsorption systems for establishment of multi-
537 bed and/or multi-stage strategies, and (iv) Optimizing operating parameters of the adsorption
538 systems depending upon the available waste heat and/or renewable energy options.
539



540
541 **Fig. 15.** COP trend of conventional adsorbent based cooling system and improvement with
542 advance MOFs development. The adsorbents used for this comparison are referred from following
543 studies [8,10,17–19,27,28,34,37,41,49,70,74,78,87,88,129,135–144,147–151,157,158,168–170].
544

545 5. Conclusions

546 Metal-organic frameworks (MOFs) or porous coordination polymers are a highly porous class
547 of adsorbents with excellent structural and water-vapor adsorptive properties. These are new micro
548 to nano porous class of adsorbent with great potential to develop energy-efficient thermally driven
549 adsorption systems/technologies. The hydrophilic MOF adsorbents are critically studied in the
550 literature for the development of various adsorption-based applications. Thereby, this study
551 provides a comprehensive review of various hydrophilic MOF adsorbents concerning crystal
552 formation, structural stability, water-vapor adsorption equilibrium, adsorption chemistry, and

553 associated potential applications, i.e. cooling, air-conditioning, and water distillation/harvesting.
554 Furthermore, a comprehensive comparison of the coefficient of performance between the studied
555 MOFs and conventional adsorbents is developed for the years 1975 to 2020. It has been found that
556 the majority of the MOFs based adsorption systems provide considerably higher performance as
557 compared to most of the conventional adsorbents-based systems. The study concludes that the
558 MOF based systems are coming strongly to the commercial market, and we may soon see one of
559 these systems sold commercially. The insights of the conclusions are as follows:

560 Zinc-based MOFs are not stable in the presence of water-vapors due to Zn metal's sensitivity
561 to water molecules, e.g. MOF-5 is not stable when water contents are more than 4%. Zirconium-
562 based MOFs are found relatively more stable in the presence of water-vapors; however, adsorption
563 uptake for most of the adsorbents of this category is quite low. In this regard, UiO-66 with
564 micropores possesses water-vapor adsorption uptake of 0.4 kg/kg at 25°C and saturation condition.
565 However, it has no cyclic stability, and the adsorption ability is perceptibly reduced after
566 continuous cyclic use, limiting its usage. On the other hand, MOF-801 and MOF-841 show
567 maximum uptake of 0.32 kg/kg and 0.53 kg/kg, respectively, at 25°C (saturation condition). The
568 MOF-801 is found a promising candidate for air-conditioning application due to cyclic stability.
569 It also shows good results for water harvesting application with maximum water production of
570 0.19 L/kg (considering kinetics losses) at a relative humidity of 40% and a regeneration
571 temperature of 85°C. Nickel-based CPO-27 is found stable in the presence of water-vapors and
572 provides type-I adsorption isotherm according to IUPAC classification with the uptake of 0.47
573 kg/kg (at saturation). It possesses cyclic stability and gives COP of 0.45 for automotive air-
574 conditioning application. It provides specific daily water production of 22.8 m³/tonne.ads/day and
575 cooling effect of 215.99 Rton/tonne in case of water desalination application for inlet temperature
576 of 40°C (condenser) and 5°C (evaporator). Copper-based HKUST-1 results adsorption uptake of
577 0.55 kg/kg at 25°C (saturation condition). It is a promising candidate for air-conditioning
578 application, whereas its stability reduces at a high relative pressure range due to Cu-Cu bond length
579 elongation.

580 On the other hand, MIL series-based MOFs possess stable structures and exhibit adsorption
581 isotherms of type-IV and type-V. In this regard, MIL-101(Cr) possesses the highest water-vapor
582 adsorption uptake (i.e. 1.45 kg/kg at 25°C on saturation condition) compared to the studied MOFs.
583 Based on the reported results, it performed better in air-conditioning, single-/ two-bed desalination

584 and heat transformation applications/systems. It also shows good performance with different
585 refrigerants other than water, e.g. ethanol and methanol. Besides, adsorption uptake can also
586 increase from 1.45 to 1.6 kg/kg when coated with graphite oxide. Similarly, MIL-53(Al) exhibits
587 specific daily water production of 25.5 m³/ton.day (maximum) with a specific cooling power of
588 789.4 W/kg in water desalination application. It has been found that MIL-101(Cr) and MIL-53(Al)
589 are promising hydrophilic MOFs which can be considered for various water adsorption-based
590 applications.

591

592 **CRedit authorship contribution statement**

593 **Sahrish Ashraf:** Conceptualization, Methodology, Software, Formal analysis, Investigation,
594 Writing - Original Draft. **Muhammad Sultan:** Conceptualization, Methodology, Validation,
595 Resources, Writing - Review & Editing, Visualization, Supervision, Project administration,
596 Funding acquisition. **Majid Bahrami:** Validation, Resources, Writing - Review & Editing,
597 Supervision, Project administration, Funding acquisition. **Claire McCague:** Data Curation,
598 Writing - Review & Editing, Visualization. **Muhammad W. Shahzad:** Formal analysis, Writing
599 - Review & Editing, Visualization. **Mohammad Amani:** Software, Writing - Review & Editing,
600 Visualization. **Redmond R. Shamschiri:** Data Curation, Writing - Review & Editing,
601 Visualization.

602

603 **Declaration of Competing Interest**

604 The authors declare that they have no known competing financial interests or personal
605 relationships that could have appeared to influence the work reported in this paper.

606

607 **Acknowledgements**

608 This research was carried out with the financially supported of Bahauddin Zakariya University,
609 Multan-Pakistan under the Director Research/ ORIC grant entitled "Investigation of agriculture
610 based low-cost ad/sorbents for desiccant air-conditioning applications" awarded to Principal
611 Investigator Dr. Muhammad Sultan.

612

613 **References**

- 614 [1] Sultan M, El-Sharkawy II, Miyazaki T, Saha BB, Koyama S. An overview of solid
615 desiccant dehumidification and air conditioning systems. *Renew Sustain Energy Rev*
616 2015;46:16–29. <https://doi.org/10.1016/j.rser.2015.02.038>.
- 617 [2] Choudhury B, Saha BB, Chatterjee PK, Sarkar JP. An overview of developments in
618 adsorption refrigeration systems towards a sustainable way of cooling. *Appl Energy*
619 2013;104:554–67. <https://doi.org/10.1016/j.apenergy.2012.11.042>.
- 620 [3] Younes MM, El-Sharkawy II, Kabeel AE, Saha BB. A review on adsorbent-adsorbate
621 pairs for cooling applications. *Appl Therm Eng* 2017;114:394–414.
622 <https://doi.org/10.1016/j.applthermaleng.2016.11.138>.
- 623 [4] Pan QW, Wang RZ. Study on boundary conditions of adsorption heat pump systems using
624 different working pairs for heating application. *Energy Convers Manag* 2017;154:322–35.
625 <https://doi.org/10.1016/j.enconman.2017.11.023>.
- 626 [5] Sultan M, Miyazaki T, Koyama S. Optimization of adsorption isotherm types for
627 desiccant air-conditioning applications. *Renew Energy* 2018;121:441–50.
628 <https://doi.org/10.1016/j.renene.2018.01.045>.
- 629 [6] Saha BB, Uddin K, Pal A, Thu K. Emerging sorption pairs for heat pump applications: an
630 overview. *JMST Adv* 2019. <https://doi.org/10.1007/s42791-019-0010-4>.
- 631 [7] Jiang Y, Bagheri MH, Loibl RT, Schiffres SN. Thermodynamic limits of adsorption heat
632 pumps: A facile method of comparing adsorption pairs. *Appl Therm Eng*
633 2019;160:113906. <https://doi.org/10.1016/j.applthermaleng.2019.113906>.
- 634 [8] Sakoda A, Suzuki M. Simultaneous transport of heat and adsorbate in closed type
635 adsorption cooling system utilizing solar heat. *J Sol Energy Eng Trans ASME*
636 1986;108:239–45. <https://doi.org/10.1115/1.3268099>.
- 637 [9] Askalany AA, Salem M, Ismael IM, Ali AHH, Morsy MG, Saha BB. An overview on
638 adsorption pairs for cooling. *Renew Sustain Energy Rev* 2013;19:565–72.
639 <https://doi.org/10.1016/j.rser.2012.11.037>.
- 640 [10] Critoph RE, Vogel R. Possible adsorption pairs for use in solar cooling. *Int J Ambient*
641 *Energy* 1986;7:183–90. <https://doi.org/10.1080/01430750.1986.9675500>.
- 642 [11] Hamdy M, Askalany AA, Harby K, Kora N. An overview on adsorption cooling systems
643 powered by waste heat from internal combustion engine. *Renew Sustain Energy Rev*
644 2015;51:1223–34. <https://doi.org/10.1016/j.rser.2015.07.056>.
- 645 [12] Alahmer A, Ajib S, Wang X. Comprehensive strategies for performance improvement of
646 adsorption air conditioning systems: A review. *Renew Sustain Energy Rev* 2019;99:138–
647 58. <https://doi.org/10.1016/j.rser.2018.10.004>.
- 648 [13] Sultan M, Miyazaki T, Saha BB, Koyama S, Kil H-S, Nakabayashi K, et al. Adsorption of
649 Difluoromethane (HFC-32) onto phenol resin based adsorbent: Theory and experiments.
650 *Int J Heat Mass Transf* 2018;127:348–56.
651 <https://doi.org/10.1016/j.ijheatmasstransfer.2018.07.097>.
- 652 [14] Zheng X, Ge TS, Wang RZ. Recent progress on desiccant materials for solid desiccant
653 cooling systems. *Energy* 2014;74:280–94. <https://doi.org/10.1016/j.energy.2014.07.027>.
- 654 [15] Asim N, Amin MH, Alghoul MA, Badiei M, Mohammad M, Gasaymeh SS, et al. Key
655 factors of desiccant-based cooling systems: Materials. *Appl Therm Eng* 2019;159:113946.
656 <https://doi.org/10.1016/j.applthermaleng.2019.113946>.
- 657 [16] Elsayed ML, Mohammed RH, C. Chow L, Mesalhy O, Su M. Revisiting the adsorption
658 equilibrium equations of silica-gel/water for adsorption cooling applications. *Int J Refrig*

- 659 2017;86:40–7. <https://doi.org/10.1016/j.ijrefrig.2017.10.038>.
- 660 [17] Experimental investigation of a silica gel-water adsorption refrigeration cycle - the
661 influence of operating conditions on cooling output and COP — Kyushu University n.d.
662 [https://kyushu-u.pure.elsevier.com/en/publications/experimental-investigation-of-a-silica-](https://kyushu-u.pure.elsevier.com/en/publications/experimental-investigation-of-a-silica-gel-water-adsorption-refri)
663 [gel-water-adsorption-refri](https://kyushu-u.pure.elsevier.com/en/publications/experimental-investigation-of-a-silica-gel-water-adsorption-refri) (accessed January 19, 2020).
- 664 [18] Saha BB, Akisawa A, Kashiwagi T. Silica gel water advanced adsorption refrigeration
665 cycle. *Energy*, vol. 22, Elsevier Ltd; 1997, p. 437–47. [https://doi.org/10.1016/S0360-](https://doi.org/10.1016/S0360-5442(96)00102-8)
666 [5442\(96\)00102-8](https://doi.org/10.1016/S0360-5442(96)00102-8).
- 667 [19] Critoph RE. Activated carbon adsorption cycles for refrigeration and heat pumping.
668 *Carbon N Y* 1989;27:63–70. [https://doi.org/10.1016/0008-6223\(89\)90157-7](https://doi.org/10.1016/0008-6223(89)90157-7).
- 669 [20] Barton SS, Evans MJB, MacDonald JAF. The adsorption of water vapor by porous
670 carbon. *Carbon N Y* 1991;29:1099–105. [https://doi.org/10.1016/0008-6223\(91\)90026-F](https://doi.org/10.1016/0008-6223(91)90026-F).
- 671 [21] Byun J, Patel HA, Thirion D, Yavuz CT. Reversible water capture by a charged metal-free
672 porous polymer. *Polymer (Guildf)* 2017;126:308–13.
673 <https://doi.org/10.1016/j.polymer.2017.05.071>.
- 674 [22] Jia L, Yao X, Ma J, Long C. Adsorption kinetics of water vapor on hypercrosslinked
675 polymeric adsorbent and its comparison with carbonaceous adsorbents. *Microporous*
676 *Mesoporous Mater* 2017;241:178–84. <https://doi.org/10.1016/j.micromeso.2016.12.028>.
- 677 [23] Sultan M, El-Sharkawy II, Miyazaki T, Saha BB, Koyama S, Maruyama T, et al. Insights
678 of water vapor sorption onto polymer based sorbents. *Adsorption* 2015;21:205–15.
679 <https://doi.org/10.1007/s10450-015-9663-y>.
- 680 [24] Sultan M, El-Sharkawy II, Miyazaki T, Saha BB, Koyama S, Maruyama T, et al. Water
681 vapor sorption kinetics of polymer based sorbents: Theory and experiments. *Appl Therm*
682 *Eng* 2016;106:192–202. <https://doi.org/10.1016/j.applthermaleng.2016.05.192>.
- 683 [25] Hanif S, Sultan M, Miyazaki T. Effect of relative humidity on thermal conductivity of
684 zeolite-based adsorbents: Theory and experiments. *Appl Therm Eng* 2019;150:11–8.
685 <https://doi.org/10.1016/j.applthermaleng.2018.12.144>.
- 686 [26] Henninger SK, Ernst SJ, Gordeeva L, Bendix P, Fröhlich D, Grekova AD, et al. New
687 materials for adsorption heat transformation and storage. *Renew Energy* 2017;110:59–68.
688 <https://doi.org/10.1016/j.renene.2016.08.041>.
- 689 [27] Meunier F. Second law analysis of a solid adsorption heat pump operating on reversible
690 cascade cycles: Application to the Zeolite-water pair. *J Heat Recover Syst* 1985;5:133–41.
691 [https://doi.org/10.1016/0198-7593\(85\)90045-1](https://doi.org/10.1016/0198-7593(85)90045-1).
- 692 [28] Chandra I, Patwardhan VS. Theoretical studies on adsorption heat transformer using
693 zeolite-water vapour pair. *Heat Recover Syst CHP* 1990;10:527–37.
694 [https://doi.org/10.1016/0890-4332\(90\)90203-V](https://doi.org/10.1016/0890-4332(90)90203-V).
- 695 [29] Sultan M, Miyazaki T, Saha BB, Koyama S. Steady-state investigation of water vapor
696 adsorption for thermally driven adsorption based greenhouse air-conditioning system.
697 *Renew Energy* 2016;86:785–95. <https://doi.org/10.1016/j.renene.2015.09.015>.
- 698 [30] Hanif S, Sultan M, Miyazaki T, Koyama S. Investigation of energy-efficient solid
699 desiccant system for the drying of wheat grains. *Int J Agric Biol Eng* 2019;12:221–8.
700 <https://doi.org/10.25165/j.ijabe.20191201.3854>.
- 701 [31] Mahmood MH, Sultan M, Miyazaki T. Solid desiccant dehumidification-based air-
702 conditioning system for agricultural storage application: Theory and experiments. *Proc*
703 *Inst Mech Eng Part A J Power Energy* 2019:095765091986950.
704 <https://doi.org/10.1177/0957650919869503>.

- 705 [32] Lim K, Che J, Lee J. Experimental study on adsorption characteristics of a water and
706 silica-gel based thermal energy storage (TES) system. *Appl Therm Eng* 2017;110:80–8.
707 <https://doi.org/10.1016/j.applthermaleng.2016.08.098>.
- 708 [33] Lu Z, Wang R, Xia Z. Experimental analysis of an adsorption air conditioning with micro-
709 porous silica gel-water. *Appl Therm Eng* 2013;50:1015–20.
710 <https://doi.org/10.1016/j.applthermaleng.2012.07.041>.
- 711 [34] Passos E, Meunier F, Gianola JC. Thermodynamic performance improvement of an
712 intermittent solar-powered refrigeration cycle using adsorption of methanol on activated
713 carbon. *J Heat Recover Syst* 1986;6:259–64. [https://doi.org/10.1016/0198-
714 7593\(86\)90010-X](https://doi.org/10.1016/0198-7593(86)90010-X).
- 715 [35] Sitorus TB, Napitupulu FH, Ambarita H. A Study on Adsorption Refrigerator Driven by
716 Solar Collector Using Indonesian Activated Carbon. *J Eng Technol Sci* 2018;49:657.
717 <https://doi.org/10.5614/j.eng.technol.sci.2017.49.5.7>.
- 718 [36] Abdullah MO, Tan IAW, Lim LS. Automobile adsorption air-conditioning system using
719 oil palm biomass-based activated carbon: A review. *Renew Sustain Energy Rev*
720 2011;15:2061–72. <https://doi.org/10.1016/j.rser.2011.01.012>.
- 721 [37] Pons M, Grenier P. Experimental data on a solar-powered ice maker using activated
722 carbon and methanol adsorption pair. *J Sol Energy Eng Trans ASME* 1987;109:303–10.
723 <https://doi.org/10.1115/1.3268222>.
- 724 [38] Sultan M, Miyazaki T, Koyama S, Khan ZM. Performance evaluation of hydrophilic
725 organic polymer sorbents for desiccant air-conditioning applications. *Adsorpt Sci Technol*
726 2018;36:311–26. <https://doi.org/10.1177/0263617417692338>.
- 727 [39] Lu YZ, Wang RZ, Zhang M, Jiangzhou S. Adsorption cold storage system with zeolite-
728 water working pair used for locomotive air conditioning. *Energy Convers Manag*
729 2003;44:1733–43. [https://doi.org/10.1016/S0196-8904\(02\)00169-3](https://doi.org/10.1016/S0196-8904(02)00169-3).
- 730 [40] Restuccia G, Freni A, Maggio G. A zeolite-coated bed for air conditioning adsorption
731 systems: Parametric study of heat and mass transfer by dynamic simulation. *Appl Therm*
732 *Eng* 2002;22:619–30. [https://doi.org/10.1016/S1359-4311\(01\)00114-4](https://doi.org/10.1016/S1359-4311(01)00114-4).
- 733 [41] Ng KC, Burhan M, Shahzad MW, Ismail A Bin. A Universal Isotherm Model to Capture
734 Adsorption Uptake and Energy Distribution of Porous Heterogeneous Surface. *Sci Rep*
735 2017;7:1–11. <https://doi.org/10.1038/s41598-017-11156-6>.
- 736 [42] Evans JD, Garai B, Reinsch H, Li W, Dissegna S, Bon V, et al. Metal–organic
737 frameworks in Germany: From synthesis to function. *Coord Chem Rev* 2019;380:378–
738 418. <https://doi.org/10.1016/j.ccr.2018.10.002>.
- 739 [43] Li H, Eddaoudi M, O’Keeffe M, Yaghi OM. Design and synthesis of an exceptionally
740 stable and highly porous metal-organic framework. *Nature* 1999;402:276–9.
741 <https://doi.org/10.1038/46248>.
- 742 [44] Perry VI JJ, Perman JA, Zaworotko MJ. Design and synthesis of metal-organic
743 frameworks using metal-organic polyhedra as supermolecular building blocks. *Chem Soc*
744 *Rev* 2009;38:1400–17. <https://doi.org/10.1039/b807086p>.
- 745 [45] Elsaidi SK, Mohamed MH, Banerjee D, Thallapally PK. Flexibility in Metal–Organic
746 Frameworks: A fundamental understanding. *Coord Chem Rev* 2018;358:125–52.
747 <https://doi.org/10.1016/j.ccr.2017.11.022>.
- 748 [46] Yaghi OM, O’Keeffe M, Ockwig NW, Chae HK, Eddaoudi M, Kim J. Reticular synthesis
749 and the design of new materials. *Nature* 2003;423:705–14.
750 <https://doi.org/10.1038/nature01650>.

- 751 [47] Najafi Nobar S. Cu-BTC synthesis, characterization and preparation for adsorption
752 studies. *Mater Chem Phys* 2018;213:343–51.
753 <https://doi.org/10.1016/j.matchemphys.2018.04.031>.
- 754 [48] Alvaro M, Carbonell E, Ferrer B, Llabrés I Xamena FX, Garcia H. Semiconductor
755 behavior of a metal-organic framework (MOF). *Chem - A Eur J* 2007;13:5106–12.
756 <https://doi.org/10.1002/chem.200601003>.
- 757 [49] Elsayed E, Al-Dadah R, Mahmoud S, Elsayed A, Anderson PA. Aluminium fumarate and
758 CPO-27(Ni) MOFs: Characterization and thermodynamic analysis for adsorption heat
759 pump applications. *Appl Therm Eng* 2016;99:802–12.
760 <https://doi.org/10.1016/j.applthermaleng.2016.01.129>.
- 761 [50] Elsayed E, AL-Dadah R, Mahmoud S, Anderson PA, Elsayed A, Youssef PG. CPO-
762 27(Ni), aluminium fumarate and MIL-101(Cr) MOF materials for adsorption water
763 desalination. *Desalination* 2017;406:25–36. <https://doi.org/10.1016/j.desal.2016.07.030>.
- 764 [51] Fernandez CA, Thallapally PK, Motkuri RK, Nune SK, Sumrak JC, Tian J, et al. Gas-
765 induced expansion and contraction of a fluorinated metal-organic framework. *Cryst
766 Growth Des* 2010;10:1037–9. <https://doi.org/10.1021/cg9014948>.
- 767 [52] Youssef PG, Dakkama H, Mahmoud SM, AL-Dadah RK. Experimental investigation of
768 adsorption water desalination/cooling system using CPO-27Ni MOF. *Desalination*
769 2017;404:192–9. <https://doi.org/10.1016/j.desal.2016.11.008>.
- 770 [53] Shi B, Al-Dadah R, Mahmoud S, Elsayed A, Elsayed E. CPO-27(Ni) metal-organic
771 framework based adsorption system for automotive air conditioning. *Appl Therm Eng*
772 2016;106:325–33. <https://doi.org/10.1016/j.applthermaleng.2016.05.109>.
- 773 [54] Bahri M, Haghighat F, Kazemian H, Rohani S. A comparative study on metal organic
774 frameworks for indoor environment application: Adsorption evaluation. *Chem Eng J*
775 2017;313:711–23. <https://doi.org/10.1016/j.cej.2016.10.004>.
- 776 [55] Rezk A, Al-Dadah R, Mahmoud S, Elsayed A. Experimental investigation of metal
777 organic frameworks characteristics for water adsorption chillers. *Proc Inst Mech Eng Part
778 C J Mech Eng Sci* 2013;227:992–1005. <https://doi.org/10.1177/0954406212456469>.
- 779 [56] Grajciar L, Bludský O, Nachtigall P. Water adsorption on coordinatively unsaturated sites
780 in CuBTC MOF. *J Phys Chem Lett* 2010;1:3354–9. <https://doi.org/10.1021/jz101378z>.
- 781 [57] Rajkumar T, Kukkar D, Kim KH, Sohn JR, Deep A. Cyclodextrin-metal-organic
782 framework (CD-MOF): From synthesis to applications. *J Ind Eng Chem* 2019;72:50–66.
783 <https://doi.org/10.1016/j.jiec.2018.12.048>.
- 784 [58] Wickenheisser M, Herbst A, Tannert R, Milow B, Janiak C. Hierarchical MOF-xerogel
785 monolith composites from embedding MIL-100(Fe,Cr) and MIL-101(Cr) in resorcinol-
786 formaldehyde xerogels for water adsorption applications. *Microporous Mesoporous Mater*
787 2015;215:143–53. <https://doi.org/10.1016/j.micromeso.2015.05.017>.
- 788 [59] Wickenheisser M, Paul T, Janiak C. Prospects of monolithic MIL-
789 MOF@poly(NIPAM)HIPE composites as water sorption materials. *Microporous
790 Mesoporous Mater* 2016;220:258–69. <https://doi.org/10.1016/j.micromeso.2015.09.008>.
- 791 [60] Bareschino P, Diglio G, Pepe F, Angrisani G, Roselli C, Sasso M. Numerical study of a
792 MIL101 metal organic framework based desiccant cooling system for air conditioning
793 applications. *Appl Therm Eng* 2017;124:641–51.
794 <https://doi.org/10.1016/j.applthermaleng.2017.06.024>.
- 795 [61] Greathouse JA, Allendorf MD. The interaction of water with MOF-5 simulated by
796 molecular dynamics. *J Am Chem Soc* 2006;128:10678–9.

- 797 <https://doi.org/10.1021/ja063506b>.
- 798 [62] Ming Y, Kumar N, Siegel DJ. Water Adsorption and Insertion in MOF-5. *ACS Omega*
- 799 2017;2:4921–8. <https://doi.org/10.1021/acsomega.7b01129>.
- 800 [63] Chui SSY, Lo SMF, Charmant JPH, Orpen a G, Williams ID. A Chemically
- 801 Functionalizable Nanoporous Material [Cu₃(TMA)₂(H₂O)₃]_n. *Science* (80-
- 802 1999;283:1148–50. <https://doi.org/10.1126/science.283.5405.1148>.
- 803 [64] Díaz-garcía M, Sánchez-sánchez M. Microporous and Mesoporous Materials Synthesis
- 804 and characterization of a new Cd-based metal-organic framework isostructural with MOF-
- 805 74 / CPO-27 materials 2014;190:248–54.
- 806 <https://doi.org/10.1016/j.micromeso.2014.02.021>.
- 807 [65] Liu J, Wang Y, Benin AI, Jakubczak P, Willis RR, LeVan MD. CO₂/H₂O adsorption
- 808 equilibrium and rates on metal-organic frameworks: HKUST-1 and Ni/DOBDC.
- 809 *Langmuir* 2010;26:14301–7. <https://doi.org/10.1021/la102359q>.
- 810 [66] Teo HWB, Chakraborty A. Water Adsorption on Various Metal Organic Framework. *IOP*
- 811 *Conf Ser Mater Sci Eng* 2017;272:012019. [https://doi.org/10.1088/1757-](https://doi.org/10.1088/1757-899X/272/1/012019)
- 812 [899X/272/1/012019](https://doi.org/10.1088/1757-899X/272/1/012019).
- 813 [67] Gordeeva LG, Solovyeva M V., Aristov YI. NH₂-MIL-125 as a promising material for
- 814 adsorptive heat transformation and storage. *Energy* 2016;100:18–24.
- 815 <https://doi.org/10.1016/j.energy.2016.01.034>.
- 816 [68] Furukawa H, Gándara F, Zhang Y-B, Jiang J, Queen WL, Hudson MR, et al. Water
- 817 Adsorption in Porous Metal–Organic Frameworks and Related Materials. *J Am Chem Soc*
- 818 2014;136:4369–81. <https://doi.org/10.1021/ja500330a>.
- 819 [69] Bon V, Senkowska I, Evans JD, Wöllner M, Hölzel M, Kaskel S. Insights into the water
- 820 adsorption mechanism in the chemically stable zirconium-based MOF DUT-67-a
- 821 prospective material for adsorption-driven heat transformations. *J Mater Chem A*
- 822 2019;7:12681–90. <https://doi.org/10.1039/c9ta00825j>.
- 823 [70] Arh S, Gašperšič B. Development and comparison of different advanced absorption
- 824 cycles. *Int J Refrig* 1990;13:41–50. [https://doi.org/10.1016/0140-7007\(90\)90053-Y](https://doi.org/10.1016/0140-7007(90)90053-Y).
- 825 [71] Solovyeva M V., Aristov YI, Gordeeva LG. NH₂-MIL-125 as promising adsorbent for
- 826 adsorptive cooling: Water adsorption dynamics. *Appl Therm Eng* 2017;116:541–8.
- 827 <https://doi.org/10.1016/j.applthermaleng.2017.01.080>.
- 828 [72] Tatlier M. Performances of MOF vs. zeolite coatings in adsorption cooling applications.
- 829 *Appl Therm Eng* 2017;113:290–7. <https://doi.org/10.1016/j.applthermaleng.2016.10.189>.
- 830 [73] Kummer H, Baumgartner M, Hüggenell P, Fröhlich D, Henninger SK, Glöser R.
- 831 Thermally driven refrigeration by methanol adsorption on coatings of HKUST-1 and
- 832 MIL-101(Cr). *Appl Therm Eng* 2017;117:689–97.
- 833 <https://doi.org/10.1016/j.applthermaleng.2016.11.026>.
- 834 [74] Jenks JJ, Motkuri RK, TeGrotenhuis W, Paul BK, McGrail BP. Simulation and
- 835 Experimental Study of Metal Organic Frameworks Used in Adsorption Cooling. *Heat*
- 836 *Transf Eng* 2017;38:1305–15. <https://doi.org/10.1080/01457632.2016.1242965>.
- 837 [75] Ma L, Rui Z, Wu Q, Yang H, Yin Y, Liu Z, et al. Performance evaluation of shaped MIL-
- 838 101-ethanol working pair for adsorption refrigeration. *Appl Therm Eng* 2016;95:223–8.
- 839 <https://doi.org/10.1016/j.applthermaleng.2015.09.023>.
- 840 [76] Rezk A, AL-Dadah R, Mahmoud S, Elsayed A. Investigation of Ethanol/metal organic
- 841 frameworks for low temperature adsorption cooling applications. *Appl Energy*
- 842 2013;112:1025–31. <https://doi.org/10.1016/j.apenergy.2013.06.041>.

- 843 [77] Saha BB, El-Sharkawy II, Miyazaki T, Koyama S, Henninger SK, Herbst A, et al. Ethanol
844 adsorption onto metal organic framework: Theory and experiments. *Energy* 2015;79:363–
845 70. <https://doi.org/10.1016/j.energy.2014.11.022>.
- 846 [78] Li W, Xia X, Cao M, Li S. Structure-property relationship of metal-organic frameworks
847 for alcohol-based adsorption-driven heat pumps via high-throughput computational
848 screening. *J Mater Chem A* 2019;7:7470–9. <https://doi.org/10.1039/C8TA07909A>.
- 849 [79] Sultan M, Mahmood MH, Miyazaki T, Koyama S, Khan ZM. Close and open cycle
850 adsorption kinetics: Development of correlation for desiccant air-conditioning. *J Eng Appl*
851 *Sci* 2016;35:1–8.
- 852 [80] Burtch NC, Jasuja H, Walton KS. Water stability and adsorption in metal-organic
853 frameworks. *Chem Rev* 2014;114:10575–612. <https://doi.org/10.1021/cr5002589>.
- 854 [81] Dakkama HJ, Youssef PG, Al-Dadah RK, Mahmoud S. Adsorption ice making and water
855 desalination system using metal organic frameworks/water pair. *Energy Convers Manag*
856 2017;142:53–61. <https://doi.org/10.1016/j.enconman.2017.03.036>.
- 857 [82] Solovyeva M V., Gordeeva LG, Krieger TA, Aristov YI. MOF-801 as a promising
858 material for adsorption cooling: Equilibrium and dynamics of water adsorption. *Energy*
859 *Convers Manag* 2018;174:356–63. <https://doi.org/10.1016/j.enconman.2018.08.032>.
- 860 [83] Khutia A, Rammelberg HU, Schmidt T, Henninger S, Janiak C. Water sorption cycle
861 measurements on functionalized MIL-101Cr for heat transformation application. *Chem*
862 *Mater* 2013;25:790–8. <https://doi.org/10.1021/cm304055k>.
- 863 [84] Hastürk E, Ernst SJ, Janiak C. Recent advances in adsorption heat transformation focusing
864 on the development of adsorbent materials. *Curr Opin Chem Eng* 2019;24:26–36.
865 <https://doi.org/10.1016/j.coche.2018.12.011>.
- 866 [85] D’Ans P, Courbon E, Permyakova A, Nouar F, Simonnet-Jégat C, Bourdreux F, et al. A
867 new strontium bromide MOF composite with improved performance for solar energy
868 storage application. *J Energy Storage* 2019;25:100881.
869 <https://doi.org/10.1016/j.est.2019.100881>.
- 870 [86] Qin M, Hou P, Wu Z, Wang J. Precise humidity control materials for autonomous
871 regulation of indoor moisture. *Build Environ* 2019:106581.
872 <https://doi.org/10.1016/j.buildenv.2019.106581>.
- 873 [87] Shi B. Development of an MOF based adsorption air conditioning system for automotive
874 application 2015.
- 875 [88] Drout RJ, Robison L, Chen Z, Islamoglu T, Farha OK. Zirconium Metal–Organic
876 Frameworks for Organic Pollutant Adsorption. *Trends Chem* 2019;1:304–17.
877 <https://doi.org/10.1016/j.trechm.2019.03.010>.
- 878 [89] Kim H, Yang S, Rao SR, Narayanan S, Kapustin EA, Furukawa H, et al. Water harvesting
879 from air with metal-organic frameworks powered by natural sunlight. *Science (80-*
880 *)* 2017;356:430–4. <https://doi.org/10.1126/science.aam8743>.
- 881 [90] Entezari A, Ejeian M, Wang R. Modifying water sorption properties with polymer
882 additives for atmospheric water harvesting applications. *Appl Therm Eng*
883 2019;161:114109. <https://doi.org/10.1016/j.applthermaleng.2019.114109>.
- 884 [91] Weiss A, Reimer N, Stock N, Tiemann M, Wagner T. Screening of mixed-linker CAU-10
885 MOF materials for humidity sensing by impedance spectroscopy. *Microporous*
886 *Mesoporous Mater* 2016;220:39–43. <https://doi.org/10.1016/j.micromeso.2015.08.020>.
- 887 [92] karmakar S, Dechnik J, Janiak C, De S. Aluminium fumarate metal-organic framework: A
888 super adsorbent for fluoride from water. *J Hazard Mater* 2016;303:10–20.

- 889 <https://doi.org/10.1016/j.jhazmat.2015.10.030>.
- 890 [93] Lin KYA, Liu YT, Chen SY. Adsorption of fluoride to UiO-66-NH₂ in water:
891 Stability, kinetic, isotherm and thermodynamic studies. *J Colloid Interface Sci*
892 2016;461:79–87. <https://doi.org/10.1016/j.jcis.2015.08.061>.
- 893 [94] Yan J, Yu Y, Ma C, Xiao J, Xia Q, Li Y, et al. Adsorption isotherms and kinetics of water
894 vapor on novel adsorbents MIL-101(Cr)@GO with super-high capacity. *Appl Therm Eng*
895 2015;84:118–25. <https://doi.org/10.1016/j.applthermaleng.2015.03.040>.
- 896 [95] Férey G, Mellot-Draznieks C, Serre C, Millange F, Dutour J, Surblé S, et al. A Chromium
897 Terephthalate – Based Solid with Unusually Large Pore Volumes and Surface Area.
898 *Science* (80-) 2005;309:2040–2. <https://doi.org/10.1126/science.1116275>.
- 899 [96] Jeremias F, Fröhlich D, Janiak C, Henninger SK. Advancement of sorption-based heat
900 transformation by a metal coating of highly-stable, hydrophilic aluminium fumarate MOF.
901 *RSC Adv* 2014;4:24073–82. <https://doi.org/10.1039/c4ra03794d>.
- 902 [97] Jeremias F, Khutia A, Henninger SK, Janiak C. MIL-100(Al, Fe) as water adsorbents for
903 heat transformation purposes - A promising application. *J Mater Chem* 2012;22:10148–
904 51. <https://doi.org/10.1039/c2jm15615f>.
- 905 [98] Wickenheisser M, Jeremias F, Henninger SK, Janiak C. Grafting of hydrophilic ethylene
906 glycols or ethylenediamine on coordinatively unsaturated metal sites in MIL-100(Cr) for
907 improved water adsorption characteristics. *Inorganica Chim Acta* 2013;407:145–52.
908 <https://doi.org/10.1016/j.ica.2013.07.024>.
- 909 [99] Jeremias F, Lozan V, Henninger SK, Janiak C. Programming MOFs for water sorption:
910 Amino-functionalized MIL-125 and UiO-66 for heat transformation and heat storage
911 applications. *Dalt Trans* 2013;42:15967–73. <https://doi.org/10.1039/c3dt51471d>.
- 912 [100] Kim SN, Kim J, Kim HY, Cho HY, Ahn WS. Adsorption/catalytic properties of MIL-125
913 and NH₂-MIL-125. *Catal Today* 2013;204:85–93.
914 <https://doi.org/10.1016/j.cattod.2012.08.014>.
- 915 [101] Sindoro M, Jee AY, Granick S. Shape-selected colloidal MOF crystals for aqueous use.
916 *Chem Commun* 2013;49:9576–8. <https://doi.org/10.1039/c3cc45935g>.
- 917 [102] Cunha D, Ben Yahia M, Hall S, Miller SR, Chevreau H, Elkaïm E, et al. Rationale of drug
918 encapsulation and release from biocompatible porous metal-organic frameworks. *Chem*
919 *Mater* 2013;25:2767–76. <https://doi.org/10.1021/cm400798p>.
- 920 [103] Towsif Abtab SM, Alezi D, Bhatt PM, Shkurenko A, Belmabkhout Y, Aggarwal H, et al.
921 Reticular Chemistry in Action: A Hydrolytically Stable MOF Capturing Twice Its Weight
922 in Adsorbed Water. *Chem* 2018;4:94–105. <https://doi.org/10.1016/j.chempr.2017.11.005>.
- 923 [104] Tranchemontagne DJ, Hunt JR, Yaghi OM. Room temperature synthesis of metal-organic
924 frameworks: MOF-5, MOF-74, MOF-177, MOF-199, and IRMOF-0. *Tetrahedron*
925 2008;64:8553–7. <https://doi.org/10.1016/j.tet.2008.06.036>.
- 926 [105] Karra JR, Grabicka BE, Huang YG, Walton KS. Adsorption study of CO₂, CH₄, N₂, and
927 H₂O on an interwoven copper carboxylate metal-organic framework (MOF-14). *J Colloid*
928 *Interface Sci* 2013;392:331–6. <https://doi.org/10.1016/j.jcis.2012.10.018>.
- 929 [106] Zhao Z, Wang S, Yang Y, Li X, Li J, Li Z. Competitive adsorption and selectivity of
930 benzene and water vapor on the microporous metal organic frameworks (HKUST-1).
931 *Chem Eng J* 2015;259:79–89. <https://doi.org/10.1016/j.cej.2014.08.012>.
- 932 [107] Bonino F, Chavan S, Vitillo JG, Groppo E, Agostini G, Lamberti C, et al. Local structure
933 of CPO-27-Ni metallorganic framework upon dehydration and coordination of NO. *Chem*
934 *Mater* 2008;20:4957–68. <https://doi.org/10.1021/cm800686k>.

- 935 [108] Jiao Y, Morelock CR, Burtch NC, Mounfield WP, Hungerford JT, Walton KS. Tuning the
936 Kinetic Water Stability and Adsorption Interactions of Mg-MOF-74 by Partial
937 Substitution with Co or Ni. *Ind Eng Chem Res* 2015;54:12408–14.
938 <https://doi.org/10.1021/acs.iecr.5b03843>.
- 939 [109] Howe JD, Morelock CR, Jiao Y, Chapman KW, Walton KS, Sholl DS. Understanding
940 Structure, Metal Distribution, and Water Adsorption in Mixed-Metal MOF-74. *J Phys*
941 *Chem C* 2017;121:627–35. <https://doi.org/10.1021/acs.jpcc.6b11719>.
- 942 [110] Haque E, Jung SH. Synthesis of isostructural metal-organic frameworks, CPO-27s, with
943 ultrasound, microwave, and conventional heating: Effect of synthesis methods and metal
944 ions. *Chem Eng J* 2011;173:866–72. <https://doi.org/10.1016/j.cej.2011.08.037>.
- 945 [111] Xiao T, Liu D. The most advanced synthesis and a wide range of applications of MOF-74
946 and its derivatives. *Microporous Mesoporous Mater* 2019;283:88–103.
947 <https://doi.org/10.1016/j.micromeso.2019.03.002>.
- 948 [112] Reinsch H, Van Der Veen MA, Gil B, Marszalek B, Verbiest T, De Vos D, et al.
949 Structures, sorption characteristics, and nonlinear optical properties of a new series of
950 highly stable aluminum MOFs. *Chem Mater* 2013;25:17–26.
951 <https://doi.org/10.1021/cm3025445>.
- 952 [113] Schaate A, Roy P, Preuße T, Lohmeier SJ, Godt A, Behrens P. Porous interpenetrated
953 zirconium-organic frameworks (PIZOFs): A chemically versatile family of metal-organic
954 frameworks. *Chem - A Eur J* 2011;17:9320–5. <https://doi.org/10.1002/chem.201101015>.
- 955 [114] Roy P, Schaate A, Behrens P, Godt A. Post-synthetic modification of Zr-metal-organic
956 frameworks through cycloaddition reactions. *Chem - A Eur J* 2012;18:6979–85.
957 <https://doi.org/10.1002/chem.201103288>.
- 958 [115] Schaate A, Roy P, Godt A, Lippke J, Waltz F, Wiebcke M, et al. Modulated synthesis of
959 Zr-based metal-organic frameworks: From nano to single crystals. *Chem - A Eur J*
960 2011;17:6643–51. <https://doi.org/10.1002/chem.201003211>.
- 961 [116] Cunha D, Gaudin C, Colinet I, Horcajada P, Maurin G, Serre C. Rationalization of the
962 entrapping of bioactive molecules into a series of functionalized porous zirconium
963 terephthalate MOFs. *J Mater Chem B* 2013;1:1101–8. <https://doi.org/10.1039/c2tb00366j>.
- 964 [117] Cavka JH, Jakobsen S, Olsbye U, Guillou N, Lamberti C, Bordiga S, et al. A new
965 zirconium inorganic building brick forming metal organic frameworks with exceptional
966 stability. *J Am Chem Soc* 2008;130:13850–1. <https://doi.org/10.1021/ja8057953>.
- 967 [118] Gaudin C, Cunha D, Ivanoff E, Horcajada P, Chevé G, Yasri A, et al. A quantitative
968 structure activity relationship approach to probe the influence of the functionalization on
969 the drug encapsulation of porous metal-organic frameworks. *Microporous Mesoporous*
970 *Mater* 2012;157:124–30. <https://doi.org/10.1016/j.micromeso.2011.06.011>.
- 971 [119] Bon V, Senkowska I, Baburin IA, Kaskel S. Zr and Hf based Metal-Organic Frameworks:
972 Tracking down the polymorphism. *Cryst Growth Des* 2013;13:1231–7.
973 <https://doi.org/10.1021/cg301691d>.
- 974 [120] Perea-Cachero A, Dechnik J, Lahoz R, Janiak C, Téllez C, Coronas J. HKUST-1 coatings
975 on laser-microporated brass supports for water adsorption. *CrystEngComm*
976 2017;19:1470–8. <https://doi.org/10.1039/c6ce02490d>.
- 977 [121] Canivet J, Fateeva A, Guo Y, Coasne B, Farrusseng D. Water adsorption in MOFs:
978 Fundamentals and applications. *Chem Soc Rev* 2014;43:5594–617.
979 <https://doi.org/10.1039/c4cs00078a>.
- 980 [122] Lee K, Howe JD, Lin LC, Smit B, Neaton JB. Small-molecule adsorption in open-site

- 981 metal-organic frameworks: A systematic density functional theory study for rational
982 design. *Chem Mater* 2015;27:668–78. <https://doi.org/10.1021/cm502760q>.
- 983 [123] Nandasiri MI, Jambovane SR, McGrail BP, Schaeff HT, Nune SK. Adsorption, separation,
984 and catalytic properties of densified metal-organic frameworks. *Coord Chem Rev*
985 2016;311:38–52. <https://doi.org/10.1016/j.ccr.2015.12.004>.
- 986 [124] Fröhlich D, Pantatosaki E, Kolokathis PD, Markey K, Reinsch H, Baumgartner M, et al.
987 Water adsorption behaviour of CAU-10-H: A thorough investigation of its structure-
988 property relationships. *J Mater Chem A* 2016;4:11859–69.
989 <https://doi.org/10.1039/c6ta01757f>.
- 990 [125] Flage-Larsen E, Røyset A, Cavka JH, Thorshaug K. Band gap modulations in UiO metal-
991 organic frameworks. *J Phys Chem C* 2013;117:20610–6.
992 <https://doi.org/10.1021/jp405335q>.
- 993 [126] Reinsch H, De Vos D. Structures and properties of gallium-MOFs with MIL-53-topology
994 based on aliphatic linker molecules. *Microporous Mesoporous Mater* 2014;200:311–6.
995 <https://doi.org/10.1016/j.micromeso.2014.07.058>.
- 996 [127] Boutin A, Bousquet D, Ortiz AU, Coudert FX, Fuchs AH, Ballandras A, et al.
997 Temperature-induced structural transitions in the gallium-based MIL-53 metal-organic
998 framework. *J Phys Chem C* 2013;117:8180–8. <https://doi.org/10.1021/jp312179e>.
- 999 [128] Weber G, Bezverkhyy I, Bellat JP, Ballandras A, Ortiz G, Chaplais G, et al. Mechanism of
1000 water adsorption in the large pore form of the gallium-based MIL-53 metal-organic
1001 framework. *Microporous Mesoporous Mater* 2016;222:145–52.
1002 <https://doi.org/10.1016/j.micromeso.2015.10.003>.
- 1003 [129] AL-Dadah R, Mahmoud S, Elsayed E, Youssef P, Al-Mousawi F. Metal-organic
1004 framework materials for adsorption heat pumps. *Energy* 2019;116:356.
1005 <https://doi.org/10.1016/j.energy.2019.116356>.
- 1006 [130] Coudert FX, Ortiz AU, Haigis V, Bousquet D, Fuchs AH, Ballandras A, et al. Water
1007 adsorption in flexible gallium-based MIL-53 metal-organic framework. *J Phys Chem C*
1008 2014;118:5397–405. <https://doi.org/10.1021/jp412433a>.
- 1009 [131] Akiyama G, Matsuda R, Sato H, Hori A, Takata M, Kitagawa S. Effect of functional
1010 groups in MIL-101 on water sorption behavior. *Microporous Mesoporous Mater*
1011 2012;157:89–93. <https://doi.org/10.1016/j.micromeso.2012.01.015>.
- 1012 [132] Küsgens P, Rose M, Senkovska I, Fröde H, Henschel A, Siegle S, et al. Characterization
1013 of metal-organic frameworks by water adsorption. *Microporous Mesoporous Mater*
1014 2009;120:325–30. <https://doi.org/10.1016/j.micromeso.2008.11.020>.
- 1015 [133] Kim H, Rao SR, Kapustin EA, Zhao L, Yang S, Yaghi OM, et al. Adsorption-based
1016 atmospheric water harvesting device for arid climates. *Nat Commun* 2018;9:1–8.
1017 <https://doi.org/10.1038/s41467-018-03162-7>.
- 1018 [134] Ehrenmann J, Henninger SK, Janiak C. Water adsorption characteristics of MIL-101 for
1019 heat-transformation applications of MOFs. *Eur J Inorg Chem* 2011:471–4.
1020 <https://doi.org/10.1002/ejic.201001156>.
- 1021 [135] Meunier F. Adsorption heat powered heat pumps. *Appl Therm Eng* 2013;61:830–6.
1022 <https://doi.org/10.1016/j.applthermaleng.2013.04.050>.
- 1023 [136] Chang WS, Wang CC, Shieh CC. Experimental study of a solid adsorption cooling system
1024 using flat-tube heat exchangers as adsorption bed. *Appl Therm Eng* 2007;27:2195–9.
1025 <https://doi.org/10.1016/j.applthermaleng.2005.07.022>.
- 1026 [137] Liu Y, Leong KC. Numerical study of a novel cascading adsorption cycle. *Int J Refrig*

- 2006;29:250–9. <https://doi.org/10.1016/j.ijrefrig.2005.05.008>.
- 1028 [138] Qu TF, Wang RZ, Wang W. Study on heat and mass recovery in adsorption refrigeration
1029 cycles. *Appl Therm Eng* 2001;21:439–52. [https://doi.org/10.1016/S1359-4311\(00\)00050-](https://doi.org/10.1016/S1359-4311(00)00050-8)
1030 8.
- 1031 [139] Saha BB, Akisawa A, Kashiwagi T. Solar/waste heat driven two-stage adsorption chiller:
1032 The prototype. *Renew Energy* 2001;23:93–101. [https://doi.org/10.1016/S0960-](https://doi.org/10.1016/S0960-1481(00)00107-5)
1033 1481(00)00107-5.
- 1034 [140] Wang RZ. Performance improvement of adsorption cooling by heat and mass recovery
1035 operation. *Int J Refrig* 2001;24:602–11. [https://doi.org/10.1016/S0140-7007\(01\)00004-4](https://doi.org/10.1016/S0140-7007(01)00004-4).
- 1036 [141] Critoph RE. Forced convection adsorption cycles. *Appl Therm Eng* 1998;18:799–807.
1037 [https://doi.org/10.1016/s1359-4311\(97\)00110-5](https://doi.org/10.1016/s1359-4311(97)00110-5).
- 1038 [142] Shelton S V., Wepfer WJ, Miles DJ. Square wave analysis of the solid-vapor adsorption
1039 heat pump. *Heat Recover Syst CHP* 1989;9:233–47. [https://doi.org/10.1016/0890-](https://doi.org/10.1016/0890-4332(89)90007-0)
1040 4332(89)90007-0.
- 1041 [143] Reviewed P, Berkeley L, Cancer B. Lawrence Berkeley National Laboratory Lawrence
1042 Berkeley National Laboratory 2010:35–43.
- 1043 [144] Critoph RE. Performance limitations of adsorption cycles for solar cooling. *Sol Energy*
1044 1988;41:21–31. [https://doi.org/10.1016/0038-092X\(88\)90111-9](https://doi.org/10.1016/0038-092X(88)90111-9).
- 1045 [145] Askalany AA, Salem M, Ismail IM, Ali AHH, Morsy MG. A review on adsorption
1046 cooling systems with adsorbent carbon. *Renew Sustain Energy Rev* 2012;16:493–500.
1047 <https://doi.org/10.1016/j.rser.2011.08.013>.
- 1048 [146] Shmroukh AN, Ali AHH, Ookawara S. Adsorption working pairs for adsorption cooling
1049 chillers: A review based on adsorption capacity and environmental impact. *Renew Sustain*
1050 *Energy Rev* 2015;50:445–56. <https://doi.org/10.1016/j.rser.2015.05.035>.
- 1051 [147] Ülkü S. Adsorption heat pumps. *J Heat Recover Syst* 1986;6:277–84.
1052 [https://doi.org/10.1016/0198-7593\(86\)90113-X](https://doi.org/10.1016/0198-7593(86)90113-X).
- 1053 [148] Lenzen D, Zhao J, Ernst SJ, Wahiduzzaman M, Ken Inge A, Fröhlich D, et al. A metal–
1054 organic framework for efficient water-based ultra-low-temperature-driven cooling. *Nat*
1055 *Commun* 2019;10. <https://doi.org/10.1038/s41467-019-10960-0>.
- 1056 [149] Alrsheedi S, Saha BB, Chakraborty A, Alrsheedi S, Saha BB, Chakraborty A, et al.
1057 Performance Investigation of MOF-Ethanol Based Adsorption Cooling Cycle Carbon
1058 dioxide adsorption onto activated carbons View project Dew point evaporative cooling
1059 View project Performance Investigation of MOF-Ethanol Based Adsorption Cooling
1060 Cycle. 2016.
- 1061 [150] Zu K, Cui S, Qin M. Performance comparison between metal-organic framework (MOFs)
1062 and conventional desiccants (silica gel, zeolite) for a novel high temperature cooling
1063 system. *IOP Conf. Ser. Mater. Sci. Eng.*, vol. 609, Institute of Physics Publishing; 2019.
1064 <https://doi.org/10.1088/1757-899X/609/5/052013>.
- 1065 [151] Charoensupaya D, Worek WM. Parametric study of an open-cycle adiabatic, solid,
1066 desiccant cooling system. *Energy* 1988;13:739–47. [https://doi.org/10.1016/0360-](https://doi.org/10.1016/0360-5442(88)90106-5)
1067 5442(88)90106-5.
- 1068 [152] Xu F, Bian ZF, Ge TS, Dai YJ, Wang CH, Kawi S. Analysis on solar energy powered
1069 cooling system based on desiccant coated heat exchanger using metal-organic framework
1070 2019;177:211–21. <https://doi.org/10.1016/j.energy.2019.04.090>.
- 1071 [153] Motoasca E. *Energy Sustainability in Built and Urban Environments* 2019.
1072 <https://doi.org/10.1007/978-981-13-3284-5>.

- 1073 [154] Ng KC, Shahzad MW. Sustainable desalination using ocean thermocline energy. *Renew*
1074 *Sustain Energy Rev* 2018;82:240–6. <https://doi.org/10.1016/j.rser.2017.08.087>.
- 1075 [155] Shahzad MW, Burhan M, Ng KC. Pushing desalination recovery to the maximum limit:
1076 Membrane and thermal processes integration. *Desalination* 2017;416:54–64.
1077 <https://doi.org/10.1016/j.desal.2017.04.024>.
- 1078 [156] Shahzad MW, Burhan M, Ang L, Ng KC. Energy-water-environment nexus underpinning
1079 future desalination sustainability. *Desalination* 2017;413:52–64.
1080 <https://doi.org/10.1016/j.desal.2017.03.009>.
- 1081 [157] Mitra S, Thu K, Saha BB, Srinivasan K, Dutta P. Modeling study of two-stage, multi-bed
1082 air cooled silica gel + water adsorption cooling cum desalination system. *Appl Therm Eng*
1083 2017;114:704–12. <https://doi.org/10.1016/j.applthermaleng.2016.12.011>.
- 1084 [158] Yang K, Shi Y, Wu M, Wang W, Jin Y, Li R, et al. Hollow spherical SiO₂ micro-
1085 container encapsulation of LiCl for high-performance simultaneous heat reallocation and
1086 seawater desalination. *J Mater Chem A* 2020. <https://doi.org/10.1039/C9TA11721K>.
- 1087 [159] Shahzad MW, Ng KC, Thu K. Future sustainable desalination using waste heat: Kudos to
1088 thermodynamic synergy. *Environ Sci Water Res Technol* 2016;2:206–12.
1089 <https://doi.org/10.1039/c5ew00217f>.
- 1090 [160] Saha BB, El-Sharkawy II, Shahzad MW, Thu K, Ang L, Ng KC. Fundamental and
1091 application aspects of adsorption cooling and desalination. *Appl Therm Eng* 2016;97:68–
1092 76. <https://doi.org/10.1016/j.applthermaleng.2015.09.113>.
- 1093 [161] Thu K, Kim YD, Shahzad MW, Saththasivam J, Ng KC. Performance investigation of an
1094 advanced multi-effect adsorption desalination (MEAD) cycle. *Appl Energy*
1095 2015;159:469–77. <https://doi.org/10.1016/j.apenergy.2015.09.035>.
- 1096 [162] Shahzad MW, Thu K, Kim Y deuk, Ng KC. An experimental investigation on MEDAD
1097 hybrid desalination cycle. *Appl Energy* 2015;148:273–81.
1098 <https://doi.org/10.1016/j.apenergy.2015.03.062>.
- 1099 [163] Ng KC, Thu K, Oh SJ, Ang L, Shahzad MW, Ismail A Bin. Recent developments in
1100 thermally-driven seawater desalination: Energy efficiency improvement by hybridization
1101 of the MED and AD cycles. *Desalination* 2015;356:255–70.
1102 <https://doi.org/10.1016/j.desal.2014.10.025>.
- 1103 [164] Shahzad MW, Ng KC, Thu K, Saha BB, Chun WG. Multi effect desalination and
1104 adsorption desalination (MEDAD): A hybrid desalination method. *Appl Therm Eng*
1105 2014;72:289–97. <https://doi.org/10.1016/j.applthermaleng.2014.03.064>.
- 1106 [165] Ng KC, Thu K, Shahzad MW, Chun W. Progress of adsorption cycle and its hybrids with
1107 conventional multi-effect desalination processes. *IDA J Desalin Water Reuse* 2014;6:44–
1108 56. <https://doi.org/10.1179/2051645214y.0000000020>.
- 1109 [166] Son HS, Shahzad MW, Ghaffour N, Ng KC. Pilot studies on synergetic impacts of energy
1110 utilization in hybrid desalination system: Multi-effect distillation and adsorption cycle
1111 (MED-AD). *Desalination* 2020;477. <https://doi.org/10.1016/j.desal.2019.114266>.
- 1112 [167] Youssef P, Mahmoud S, Al-Dadah R, Elsayed E, El-Samni O. Numerical Investigation of
1113 Aluminum Fumarate MOF adsorbent material for adsorption desalination/cooling
1114 application. *Energy Procedia* 2017;142:1693–8.
1115 <https://doi.org/10.1016/j.egypro.2017.12.551>.
- 1116 [168] Hollman R, Little WA. Progress in the Development of Microminiature Refrigerators
1117 using Photolithographic Fabrication Techniques. *Refrigeration Cryogenic Sensors Electron Syst*
1118 1980.

- 1119 [169] Anyanwu EE. Review of solid adsorption solar refrigeration II:: An overview of the
1120 principles and theory. *Energy Convers Manag* 2004;45:1279–95.
1121 <https://doi.org/10.1016/j.enconman.2003.08.003>.
- 1122 [170] Saha BB, Boelman EC, Kashiwagi T. Computational analysis of an advanced adsorption-
1123 refrigeration cycle. *Energy* 1995;20:983–94. [https://doi.org/10.1016/0360-5442\(95\)00047-](https://doi.org/10.1016/0360-5442(95)00047-K)
1124 [K](https://doi.org/10.1016/0360-5442(95)00047-K).
- 1125 [171] Henninger SK, Schmidt FP, Henning HM. Water adsorption characteristics of novel
1126 materials for heat transformation applications. *Appl Therm Eng* 2010;30:1692–702.
1127 <https://doi.org/10.1016/j.applthermaleng.2010.03.028>.
- 1128 [172] Henninger SK, Habib HA, Janiak C. MOFs as adsorbents for low temperature heating and
1129 cooling applications. *J Am Chem Soc* 2009;131:2776–7.
1130 <https://doi.org/10.1021/ja808444z>.
1131